Structural insights in the GTP-driven monomerization and activation of a bacterial LRRK2 homologue using allosteric nanobodies

Christian Galicia[1,2], Giambattista Guaitoli[3], Marcus Fislage[1,2], Christian J. Gloeckner[3,4], Wim Versées[1,2]

[1] *VIB-VUB Center for Structural Biology, Pleinlaan 2, 1050 Brussels, Belgium.*
[2] *Structural Biology Brussels, Vrije Universiteit Brussel, Pleinlaan 2, 1050 Brussels, Belgium.*
[3] *German Center for Neurodegenerative Diseases (DZNE), Otfried-Müller-Str. 23, D-72076 Tübingen, Germany.*
[4] *Institute for Ophthalmic Research, Center for Ophthalmology, University of Tübingen, D-72076 Tübingen, Germany*

Abstract

The Roco proteins are a family of GTPases, characterized by the conserved presence of a Roc-COR tandem domain. These proteins entered the limelight after mutations in human LRRK2 were identified as a major cause of familial Parkinson's disease. LRRK2 is a large and complex protein combining a GTPase and protein kinase activity, and disease mutation increase the kinase activity, while presumably decreasing the GTPase activity. Although a cross-communication between both catalytic activities has been suggested, the underlying mechanisms and the regulatory role of the GTPase domain remain unknown. Recently, several structures of LRRK2 have been reported, but so far structures of Roco proteins in their activated GTP-bound state are lacking. Here, we use single particle cryo-EM to solve the structure of a simpler bacterial Roco protein (CtRoco) in its GTP-bound state, aided by the use of two conformation-specific nanobodies: Nb_{Roco1} and Nb_{Roco2}. This structure presents CtRoco in an active monomeric state, featuring very significant conformational changes compared to the previously solved nucleotide-free dimer structure. In particular, the structure shows a very large GTP-induced conformational change of the LRR domain, unleashing it from the Roc-COR domains, using the Roc-LRR linker as a hinge. Furthermore, this structure shows how Nb_{Roco1} and Nb_{Roco2} collaborate to activate CtRoco in an allosteric way. Altogether, our data provides important new insights in the activation mechanism of Roco proteins, with relevance to LRRK2 regulation, and suggest new routes for the allosteric modulation of their GTPase activity.

Introduction

The Roco proteins are a family of large multi-domain GTPases, with representatives in all domains of life (Bosgraaf & Van Haastert, 2003). The minimal domain arrangement that characterizes this family consists of a Roc (Ras of complex proteins) domain bearing the GTPase activity, followed by a COR (C-terminal of Roc) domain that can be further subdivided in a CORA and a CORB domain (Wauters et al., 2019). This protein family has attracted particular interest since the discovery that mutations in one of the four human Roco representatives, called Leucine-Rich Repeat Kinase 2 (LRRK2), are one of the major causes of familial Parkinson's disease (PD) (Paisán-Ruíz et al., 2004; Zimprich et al., 2004). Additionally, GWAS studies have also linked this gene to idiopathic PD, as well as to some other diseases such as Crohn's disease (Di Maio et al., 2018; Gilks et al., 2005; Hui et al., 2018). LRRK2 is a very large and complex protein, where the central Roc-COR domains are preceded by armadillo (ARM), ankyrin (ANK) and leucine-rich repeat (LRR) domains, and followed by a Ser/Thr protein kinase and a WD40 domain. Several Rab proteins have been identified as physiological substrates of the LRRK2 kinase domain (Liu et al., 2018; Steger et al., 2016, 2017).

PD-associated mutations in LRRK2 are concentrated in the catalytic Roc-COR and kinase domains, and commonly lead to an increase in kinase activity and - depending on the experimental set-up - a decrease in GTPase activity (Kalogeropulou et al., 2022; Lewis et al., 2007; West et al., 2005). Moreover, recent data also suggest a reciprocal cross-talk between both catalytic activities (Gilsbach et al., 2023; Störmer et al., 2023; Weng et al., 2023). Nevertheless, while the therapeutic targeting of the LRRK2 kinase domain has been a major focus of research in the last two decades, the regulation and targeting of the Roc-COR domains is only recently gaining more attention (Cogo et al., 2022; Helton et al., 2021; Park et al., 2022; Pathak et al., 2023).

The first important structural insights in the functioning of the Roc-COR domains and the associated GTPase activity came from work with a Roco protein from the bacterium

Chlorobaculum tepidum (CtRoco) (Deyaert et al., 2019; Gotthardt et al., 2008). Bacterial Roco proteins are simpler, only consisting of the core LRR-Roc-COR domains, and hence lack the kinase domain. A crystal structure of CtRoco in a nucleotide-free state agrees with earlier biophysical data, showing that CtRoco is a homodimer in the nucleotide-free state, while it monomerizes upon GTP binding and exists in a concentration-dependent monomer-dimer equilibrium in the GDP-bound state (Deyaert et al., 2019; Deyaert, Wauters, et al., 2017). A PD analogous mutation in the Roc domain of CtRoco (L487A), shifts this equilibrium towards the dimer and decreases the GTPase activity, suggesting that monomerization is a requirement for normal GTPase activity.

Recently, several cryo-EM structures of LRRK2 have provided crucial new insights in the LRRK2 function and regulation (Deniston et al., 2020; Myasnikov et al., 2021). Full-length LRRK2 (FL-LRRK2) appears as a mixture of monomers and homodimers under the experimental conditions used, allowing Myasnikov and colleagues to solve cryo-EM structures of both oligomeric states with the Roc domain bound to GDP (Myasnikov et al., 2021). Interestingly, the symmetrical homodimers are formed through a CORB-CORB interface, very similar to the one found in the CtRoco homodimer. The kinase domain is present in an inactive ("DYG out") conformation, with the LRR domain wrapping around the kinase ATP-binding cleft thereby blocking the entry of globular substrates and providing a mechanism of auto-inhibition. A manuscript recently published on BioRxiv reports the structure of FL-LRRK2 bound to Rab29 (Zhu et al., 2022). In addition to kinase-inactive monomers and dimers, an intriguing third form is observed in this study where LRRK2 adopts an asymmetric dimer of dimers. Each of the constituting dimers contains one protomer displaying the kinase in an inactive form and one in an active form. In the kinase-active protomer, the N-terminal (ARM-ANK-LRR) domains become flexible, thus releasing the auto-inhibition provided through the LRR domain. These data thus put forward the LRR domain as an important regulatory element. Nevertheless, while we now have access to structures of full length Roco proteins in the nucleotide-free form (CtRoco) and bound to GDP (FL-LRRK2), no structural

data is available for any Roco protein bound to GTP, leaving the role of the Roc domain and of GTP binding in the regulation of Roco proteins enigmatic.

Nanobodies (Nbs), the single domain fragments derived from camelid heavy-chain antibodies, form excellent tools to allosterically modify the activity of proteins and enzymes, including LRRK2 (Singh et al., 2022; Uchański et al., 2020). Previously, we generated two Nbs (Nb_{Roco1} and Nb_{Roco2}) that bind preferentially to the monomeric GTP-bound form of CtRoco (Leemans et al., 2020). Correspondingly, binding of Nb_{Roco1} shifts the dimer-monomer equilibrium to the monomeric state and thereby reverts the decrease in GTPase activity caused by the L487A PD-analogous mutation. However, the mechanism underlying this allosteric modulation provided by Nb_{Roco1} and Nb_{Roco2} is not yet understood.

Here we use single particle cryo-EM to solve the structure of full-length CtRoco in its GTP-state, stabilized by the binding of Nb_{Roco1} and Nb_{Roco2}. This structure presents CtRoco in an active monomeric state, featuring very significant conformational changes compared to the dimer structure. These results provide important new insights in the activation mechanism and regulation of Roco proteins, and present potential routes for the allosteric modulation of their GTPase activity.

Results

Cryo-EM structures of nanobody-stabilized CtRoco in the GTP-state reveal a monomeric "open" conformation

While we previously showed that CtRoco undergoes a dimer to monomer transition during its GTPase cycle (Deyaert, Wauters, et al., 2017) (**Figure 1A**), so far only an X-ray crystal structure of the nucleotide-free dimeric state of the protein is available. This structure shows CtRoco as a rather compact dimer where the LRR domains fold back on the Roc-COR domains (**Figure 1B**) (Deyaert et al., 2019). Obtaining well-diffracting crystals of the GTP-bound CtRoco protein is most likely hampered by the high internal flexibility of the protein, as suggested by SAXS experiments

(Deyaert, Wauters, et al., 2017). To reduce this flexibility and stabilize the protein in the monomeric GTP-bound state, we reasoned we could make use of two conformation-specific Nanobodies (Nb_{Roco1} and Nb_{Roco2}) that preferentially bind the CtRoco GTP-state (Leemans et al., 2020).

For cryo-EM sample and grid preparation, the nucleotide-free full-length CtRoco protein was incubated with an excess of the non-hydrolyzable GTP analog GTPγS and with either Nb_{Roco1} (CtRoco-Nb_{Roco1}) or with both Nb_{Roco1} and Nb_{Roco2} (CtRoco-Nb_{Roco1}-Nb_{Roco2}), and the complexes were purified using size exclusion chromatography. Cryo-EM data was collected for both complexes and map reconstructions of CtRoco-Nb_{Roco1} and CtRoco-Nb_{Roco1}-Nb_{Roco2} were refined to 8.3 Å and 7.7 Å, respectively (**Figure 1C, Figure 1–figure supplements 1 and 2, Table 1**). Both resulting maps clearly show CtRoco in a monomeric and elongated "open" conformation, in contrast to the more globular dimeric "closed" conformation previously observed in the nucleotide-free CtRoco crystal structure. Difficulties in aligning particles during data processing reflects the high flexibility of the N-terminal LRR domain vis-à-vis the C-terminal domains. This can be observed in the 2D classes from both data sets: while some display the full particle, most classes center on one half of the protein with the other half fading away as a result of flexibility. The majority of the 2D classes center on the N-terminal LRR domain and a few on the C-terminal Roc-COR domains (**Figure 1–figure supplement 3**). Similarly, 3D classification of the CtRoco-Nb_{Roco1}-Nb_{Roco2} data set produced only one class representing a nearly full reconstruction, but multiple classes centering on the LRR domain with deficient density for the rest of the protein (**Figure 1–figure supplement 1**). Further refinement with particles that converged in visible density for both domains resulted in the rather low resolution map reconstructions for the entire protein. To avoid these issues linked to inter-domain flexibility, and to increase the quality of the local reconstruction of each domain, we created focused maps from the CtRoco-Nb_{Roco1}-Nb_{Roco2} data set by processing separately the N-terminal and the C-terminal centered classes, which produced map reconstructions with mean resolutions of 3.6 Å and 3.9 Å, respectively (**Figure 1C, Figure 1–figure supplement 1, Table 1**). These focused

maps were used for all further interpretation and model building, and were finally fitted on the 7.7 Å map reconstruction of the (nearly) full protein reconstruction to create a composite map showing the relative orientation of these domains to each other (**Figures 1C and 1D**). This resulted in a good quality interpretable map for the LRR domain bound to Nb_{Roco2}, with unambiguous density for most amino acid side chains on the LRR-Nb_{Roco2} interface (**Figure 1–figure supplement 4A**). No density can be assigned to a peptide region linking the LRR domain to the Roc domain, in agreement with the flexible nature of this linker. The quality of the map for the C-terminal part of the protein is more variable. For the Roc domain unambiguous density allowing side chain interpretation is observed for some parts of the domain, including parts of the region that interacts with Nb_{Roco1}. However, while the density for GTPγS and for a large part of the Switch 2 loop could be well interpreted (**Figure 1–figure supplement 4B**), the density is ambiguous in some regions around the GTP-binding pocket and absent for most of the Switch 1 loop. The map also allows to unambiguously place Nb_{Roco1}, although it is generally of lower quality in this region. In particular, the CDR loops of Nb_{Roco1} could be identified but hardly any side chains could be assigned (**Figure 1–figure supplement 4C**). Also for the CORA and CORB domains, the quality of the map is variably spread. No density is observed for C-terminal residues of CORB (a.a. 892-940), which are involved in CtRoco dimerization. This is in very good agreement with previous hydrogen-deuterium exchange (HDX) experiment showing that this region becomes highly flexible upon GTP-driven monomerization (Deyaert et al., 2019). Nevertheless, some weak density for this region can be observed in the full reconstruction map (**Figure 1–figure supplement 1**). Finally, no density is observed for last the 150 residues of CtRoco, although on the CtRoco-Nb_{Roco1} map some additional density is observed that can account for the C-terminal region. This region is probably highly flexible and also needed to be removed to obtain diffracting crystals of the nucleotide-free CtRoco dimer (Deyaert, Kortholt, et al., 2017). Taken together, the GTPγS-bound CtRoco-Nb_{Roco1}-Nb_{Roco2} structure clearly shows the protein in a monomeric and elongated "open" conformation,

allowing us to interpret the GTP-driven conformational changes, as well as the binding sites and the mechanism of allosteric activation of Nb_{Roco1} and Nb_{Roco2} (**Figure 1D**). Only data from CtRoco-Nb_{Roco1}-Nb_{Roco2} were used for detailed analyses and will be discussed further.

GTP-mediated "activation" of CtRoco induces large-scale conformational changes linked to monomerization

Comparison of the current structure of monomeric GTPγS-bound CtRoco-Nb_{Roco1}-Nb_{Roco2} with the previously solved structure of dimeric CtRoco in the nucleotide-free (NF) state (Deyaert et al., 2019) allows us to dissect in detail the conformational changes associated with CtRoco monomerization and activation. To achieve this, protomers of each structure were superposed using their Roc domains as a reference. The most prominent conformational change concerns the position of the LRR domain. In the GTPγS-bound structure, the LRR rotates away from the Roc-COR domains by about 135° (**Figure 2A**). The hinge point for this large movement is the linker region between the LRR and Roc domains, and in particular the so-called α_0-helix that precedes the actual Roc domain. This helix is a conserved structural element of the Roco proteins, including LRRK2. In the inactive dimeric CtRoco, the α_0-helix is structurally inserted between the LRR and CORA domains, forming hydrophobic and electrostatic interactions with both domains (**Figure 2B**). However, upon GTPγS binding this helix detaches and becomes entirely solvent exposed, as such disrupting the interaction between the LRR and Roc-COR domains. This observation is in good agreement with our earlier HDX data, which also suggested that the region connecting the LRR and Roc domain becomes solvent exposed in the GTP-bound monomer (Deyaert et al., 2019).

Comparison of the Roc domains in the nucleotide-free and GTPγS-bound states, reveals a number of conformational changes. A remarkable feature of the CtRoco dimer structure was the dimer-stabilized orientation of the P-loop, which would hamper direct nucleotide binding on the dimer. Correspondingly, in the current structure the P-loop changes orientation allowing GTPγS to bind, although the EM map does not allow unambiguous placement of the entire P-loop. Surprisingly,

also the Switch 1 loop could not be fully modeled, which could indicate some flexibility in this region despite the presence of a GTP analogue. A second region of conformational change regards Switch 2. The EM map in this region and for the preceding interswitch β-strand is of reasonably good quality, allowing to model a large part of the backbone of Switch 2 (including the DxxG motif) (**Figure 2C**). Compared to the position of the nucleotide-free structure, the Switch 2 shifts to a position much closer to the P-loop which is not compatible with the dimeric arrangement of nucleotide-free CtRoco since it would sterically clash with the adjacent protomer (**Figure 2D**). Hence, those conformational changes in the P-loop and Switch 2 region could form an initial trigger for nucleotide-induced monomerization. A final important observation in the Roc domain concerns the very C-terminal part of Switch 2 (residues 520 to 533), which could not be modeled in our GTP bound structure due to flexibility, while in the nucleotide-free dimer structure this region is structured and located at the interface of the Roc domain with the LRR-Roc linker and CORA. In this way, the conformational changes induced by GTPγS binding could be relayed via the Switch 2 toward the LRR and CORA domains, and *vice versa*. On the other hand, only relatively small changes are observed in the orientation of the Roc α3 helix. This helix, which was previously suggested to be an important element in the activation of LRRK2 (Kalogeropulou et al., 2022), is located at the interface of the Roc and CORB domains and harbors the residues H554 and Y558, orthologous to the LRRK2 PD mutation sites N1337 and R1441, respectively.

In addition to the C-terminal dimerization part of CORB that becomes unstructured, also other large conformational changes are observed in the CORA and CORB domains of CtRoco upon GTPγS binding. The most prominent change in CORA concerns a shift of its N-terminal part (residues 626-693) towards a position that is incompatible with the position of the LRR and the Roc-LRR linker region in the CtRoco dimer structure (**Figure 2B**). In particular, the third helix of CORA (residues 666-678) would form sterical clashes with the α_0-helix that links the LRR and Roc domains, thus linking the conformational changes in CORA to those in the α_0-helix and LRR domain. The

displacements occurring in CORB are even more pronounced. In the GTPγS-bound monomer, the N-terminal part of CORB (residues 798 - 891) undergoes a global rotational movement of about 30° in the direction of the dimer interface of the nucleotide-free dimer (**Figure 2E, Figure 2–figure supplement 1**). Such an orientation would be incompatible with the dimeric arrangement observed in the nucleotide-free state due to severe steric clashes with the Roc domain of the adjacent subunit. Interestingly, this rotational movement of CORB seems to use the H554-Y558-Y804 triad on the interface of Roc and CORB as a pivot point (**Figure 2E**). Mutation of either of the corresponding residues in LRRK2 (N1437, R1441, Y1699, respectively) is associated with PD and leads to LRRK2 activation. Comparison of the GTPγS-bound CtRoco monomer with the nucleotide-free dimer thus clearly provides several intertwined pathways linking GTP binding to monomerization and large-scale intra-subunit conformational changes.

Nb_{Roco1} and Nb_{Roco2} allosterically lock CtRoco in its active conformation

We previously showed that Nb_{Roco1} binds CtRoco in a conformation-specific way, with highest affinity for the GTP-bound state, while no binding was observed on the nucleotide-free CtRoco dimer. As a result, Nb_{Roco1} shifts the CtRoco dimer-monomer equilibrium toward the monomeric state and increases the GTPase activity (Leemans et al., 2020). Albeit less pronounced, a similar specificity for the GTP-bound state of CtRoco is observed for Nb_{Roco2}. The current structure of GTPγS-bound CtRoco in complex with both Nb_{Roco1} and Nb_{Roco2} now reveals the mechanism underlying this conformational specificity.

Nb_{Roco1} binds to CtRoco on the interface of the Roc and CORA domains and the hinge region connecting the LRR to the Roc domain (including the α_0-helix). As such it is strategically positioned to "monitor" the nucleotide-induced conformational changes occurring in CtRoco and to stabilize the active conformation (**Figures 1D and 3A**). Specifically, the CDR1 loop of Nb_{Roco1} is within relatively close distance to the linker region connecting the LRR domain to the Roc domain,

although the local resolution in this area does not allow unequivocal placement of the residue side chains. The CDR2 loop mainly interacts with the Roc domain, including the interswitch region, while it can potentially also interact with the C-terminal end of the LRR-Roc linker. The CDR3 loop interacts with the region linking the Roc domain to CORA (**Figure 3A**). This binding mode of Nb_{Roco1} would clearly be incompatible with binding to CtRoco in its inactive nucleotide-free dimeric state. Indeed, superposition of the current structure on the CtRoco dimer shows severe sterically overlap between the Nb_{Roco1} CDR3 and the LRR, Roc and LRR-Roc linker of the CtRoco dimer, and, to a lesser extent, also between CDR1 and the LRR-Roc linker (**Figure 3B**). Hence, binding of Nb_{Roco1} to CtRoco would be expected to induce a conformational switch toward the open active state, explaining the observed preference for the GTP-bound monomeric conformation.

In the density map Nb_{Roco2} can easily be identified and placed on the concave side of the LRR domain. The main interactions occur between the CDR2 loop and the first two repeats of the LRR domain, and, in particular, between the CDR3 loop and the central region of the LRR (repeats 5-10). From CDR1, only K27 seems to be involved in the binding, by making interactions with E243 and Q245 in repeat 11 of the LRR domain. Apart from these contributions of the CDR loops, also framework residues of Nb_{Roco2} are implicated in the interaction with CtRoco, with in particular its N-terminal and C-terminal β-strands interacting with the very C-terminal repeat of the LRR. When superposing the active and inactive conformations of CtRoco, one can immediately appreciate that the placement of Nb_{Roco2} is incompatible with the LRR conformation in the inactive nucleotide-free state (**Figure 3C)**. In the latter state, the LRR folds back on the COR domains and interacts with the CORB through its repeats 9-11. Hence, this provides a mechanism for the conformational specificity of Nb_{Roco2}. Nevertheless, we previously found that Nb_{Roco2} does bind to nucleotide-free CtRoco, albeit with a lower affinity compared to the GTP state (Leemans et al., 2020). This indicates some flexibility in the position of the LRR domain, regardless of the CtRoco nucleotide state, with Nb_{Roco2} playing a more subtle role in shifting the equilibrium toward the monomeric open

conformation. The latter is in agreement with our observation that the elongated open CtRoco conformation is also observed as the main species in the CtRoco-Nb_{Roco1} structure in the absence of Nb_{Roco2} (**Figure 1–figure supplement 2**).

Cross-linking MS experiments confirm the Nb binding sites and the induced conformational changes

To further complement and confirm our structural data, we subsequently used cross-linking mass spectrometry (CX-MS) to map the Nb-induced conformational changes in CtRoco, as well as the binding sites of Nb_{Roco1} and Nb_{Roco2}. Hereto, we used the lysine-specific and CID-cleavable crosslinker DSSO (disuccinimidyl sulfoxide) (Kao et al., 2011). Considering the length of the DSSO spacer and the lysine side chains, the theoretical upper limit for the distance between the α carbon atoms of cross-linked lysines is ~26 Å, while also taking protein dynamics into account leads to a cut-off distance of 35 Å, thus also allowing to draw inter- and intramolecular interactions within this resolution limit (Erzberger et al., 2014; Kao et al., 2011). CX-MS was applied to GTPγS-bound CtRoco either in absence of Nbs, or bound to Nb_{Roco1}, Nb_{Roco2} or both Nbs. Overall, the obtained crosslinking data for the proteins in solution correspond well with the cryo-EM structures and previous biochemical data. In the GTPγS-bound CtRoco protein, in absence of Nbs, still a considerable number of cross-links are observed between the LRR domain and the other CtRoco domains, illustrating the dynamical nature of this protein state, where the LRR most probably samples both the "open" and "closed" states (**Figure 4A)**. The number of crosslinks between the LRR domain and the other protein domains is strongly decreased upon binding of either of the two Nbs, indicating that they stabilize the open conformation of CtRoco (**Figure 4A-C**). This is most prominent for Nb_{Roco1} in agreement with the strong conformational specificity of this Nb. Interestingly, in presence of both Nb_{Roco1} and Nb_{Roco2}, all the crosslinks between the LRR and C-terminal domains are lost, suggesting an additive effect of both Nbs in stabilizing the CtRoco

open conformation (**Figure 4D**). Also multiple crosslinks between the Nbs and CtRoco, as well as between both nanobodies were found. According to the cryo-EM structure Nb_{Roco1} binds to the LRR-Roc interface, and crosslinks were accordingly observed between Nb_{Roco1}-K69 and residue K443 in the LRR-Roc (α_0) linker region. Nb_{Roco1}-K69 also forms crosslinks with two lysines within the Roc domain (K583 and K611), and Nb_{Roco1}-K91 is crosslinked to K583 (**Figure 4B**). However, surprisingly, no cross-links were observed between Nb_{Roco2} and the LRR domain, while the cryo-EM structure and previous biochemical data unambiguously show binding to the LRR (Leemans et al., 2020). This can be explained by the compact folding of the LRR domain, which allows only very little rotational freedom for the lysine residues and causes a poor coverage by crosslinking data, as previously observed (Guaitoli et al., 2016).

Nb_{Roco1} and Nb_{Roco2} have a synergistic effect

While Nb_{Roco1} and Nb_{Roco2} both bind to CtRoco in a conformation-specific way, with preference for the monomeric GTP-bound conformation, this feature is most pronounced in Nb_{Roco1} for which we previously could not detect any binding to the nucleotide-free CtRoco dimer (Leemans et al., 2020). The current cryo-EM structure shows that binding of Nb_{Roco2} to nucleotide-free CtRoco must necessarily evoke a conformational change of the LRR. If this conformational change is relevant for the CtRoco activation mechanism and monomerization, we reasoned that binding of Nb_{Roco2} might sufficiently weaken the CtRoco closed conformation to allow subsequent binding of Nb_{Roco1}. To test this hypothesis, we titrated FITC labeled Nb_{Roco1} with increasing concentrations of nucleotide-free CtRoco that was pre-incubated with an excess of Nb_{Roco2}, and we followed the binding using fluorescence anisotropy measurements (**Figure 5A**). This shows that the presence of Nb_{Roco2} enables Nb_{Roco1} to bind to CtRoco in absence of nucleotides, with a $K_D = 4.6 \pm 1.6$ μM. Hence, this clearly demonstrates a synergistic effect of both Nbs in inducing conformational changes that drive CtRoco toward the active monomeric state.

A bi-valent Nb_{Roco1}-Nb_{Roco2} construct (Nb_{R2-R1}) acts as a strong activator of CtRoco

Considering the mutual synergistic effect of Nb_{Roco1} and Nb_{Roco2}**,** we reasoned that a bi-valent / bi-paratopic Nanobody construct that covalently links Nb_{Roco1} to Nb_{Roco2} would further increase the affinity and avidity towards CtRoco. Based on our cryo-EM structure, we linked the C-terminal end of Nb_{Roco2} to the N-terminus of Nb_{Roco1} using a $(GGGGS)_3$ linker, hence obtaining the bi-paratopic construct Nb_{R2-R1}. As could be expected Nb_{R2-R1} shows binding to nucleotide-free CtRoco with a K_d = 0.25 ± 0.05 μM (**Figure 5B**). This affinity of the bi-paratopic construct is 3-fold higher than that of Nb_{Roco2} alone, and even 18-fold higher than that of Nb_{Roco1} in presence of an excess of Nb_{Roco2}. Thus, this clearly shows the cooperative effect of both Nbs in the bi-paratopic construct with regard to binding and inducing conformational changes in CtRoco.

Next, we wondered whether both Nbs would also cooperate in increasing the GTPase activity of CtRoco. Indeed, we previously showed that Nb_{Roco1} increases the GTPase activity of the slow CtRoco-L487A mutant (Leemans et al., 2020). L487 is located in the Roc Switch 1 loop and the mutation is orthologous to the I1371V PD mutation in LRRK2 (Jagtap et al., 2022; Paisán-Ruíz et al., 2005). Therefore, we first performed single turnover GTPase experiments by mixing 5 μM CtRoco-L487A with 5 μM GTP in presence of an excess of both Nb_{Roco1} and Nb_{Roco2}. In presence of both Nbs the hydrolysis rate was increased 4-fold compared to CtRoco-L487A alone and 2-fold compared to CtRoco-L487A in presence of Nb_{Roco1} only, again illustrating a collaboration between the Nbs (**Figure 5C**). Finally, the single turn-over experiment was performed in the presence of the bi-paratopic Nb_{R2-R1}. Interestingly, Nb_{R2-R1} increases the GTPase turnover rate up to a level where it becomes too fast to determine an accurate k_{obs} value. Indeed, while it takes the L487A mutant more than one hour to convert all the GTP under the conditions used, in the presence of Nb_{R2-R1} nearly all the GTP has been hydrolyzed at the earliest possible sample point (20 seconds) (**Figure 5D**). This

clearly illustrates the very strong cooperative activating effect of Nb_{Roco1} and Nb_{Roco2} within the bi-paratopic construct.

Discussion

In the current study we present, to the best of our knowledge, the first structure of a protein belonging to the Roco family in a GTP-bound state, allowing us to analyze the conformational changes linked to nucleotide binding. While most attention has been devoted to human LRRK2 due to its link with PD, we used a bacterial homologue from the bacterium *C. tepidum* (CtRoco), which consists of the LRR, Roc and COR (CORA / CORB) domains, followed by a C-terminal region of about 150 residues with unknown structure. Although this protein lacks the important kinase domain, it has proven to be an excellent model to study the properties of the generally conserved core LRR-Roc-COR domains that bear the GTPase activity, revealing the GTPase-driven dimer-monomer cycle and the kinetics of GTP hydrolysis (Deyaert, Wauters, et al., 2017; Wauters et al., 2018). Previously, we solved an X-ray crystal structure of this protein in its nucleotide-free state, which displayed a compact dimeric arrangement with the LRR domain folding back on the Roc-COR domains within each protomer. Thus far, however, we had failed to produce well-diffracting crystals of this protein in a GTP-bound state, most probably due to the high dynamic nature of the protein. To decrease this flexibility, we have now used two previously developed conformation-specific nanobodies (Nb_{Roco1} and Nb_{Roco2}) to stabilize the protein in the GTP-state, allowing us to solve its structure using cryo-EM **(Figure 1)** (Leemans et al., 2020).

In accordance with biochemical studies and data from HDX-MS and negative stain EM (Deyaert et al., 2019; Deyaert, Wauters, et al., 2017), the cryo-EM structure shows the GTPγS-bound CtRoco as an elongated monomer, where the LRR domain has undergone a 135° rotation away from the Roc and COR domains. Comparison of the nucleotide-free CtRoco dimer with the GTPγS-bound monomer suggests a direct and reciprocal link between monomerization and the conformational

changes within the protomers, and allows us to propose several concerted mechanisms linking both events **(Figure 2)**. An initial trigger for monomerization seems to be the reorganization of the P-loop and Switch 2 region upon nucleotide binding, which is incompatible with the Roc:Roc dimer interface that is observed in the crystal structure of the nucleotide-free CtRoco. Via the Switch 2 loop the conformational changes can be relayed, via the region linking the LRR with the Roc domain and the CORA, toward CORB **(Figure 2)**. Specifically, in the GTP-state the CORB domain makes a 30° rotational movement in the direction of the CORB-CORB dimer interface of the CtRoco dimer. Such an orientation would result in severe steric clashes with the Roc domain of the adjacent protomer, which probably forms the major driving force for nucleotide-induced monomerization (**Figure 2**). Interestingly, the pivot point for the CORB rotational movement coincides with the hydroxyl group of Y804, which forms H-bonds with H554 and Y558 within helix α3 of the Roc domain **(Figure 2)**. H554, Y558 and Y804 correspond to N1437, R1441 and Y1699 in LRRK2, respectively, and mutation of either of these 3 residues is associated with PD and LRRK2 kinase activation (Kalogeropulou et al., 2022). In LRRK2 a "seesaw-like" movement of the α3 helix of Roc with respect to the CORB domain was observed upon activation by Rab29, and the N1437-R1441-Y1699 triad was proposed as a central region in the activation mechanism of LRRK2 (Störmer et al., 2023; Zhu et al., 2022). This thus illustrates that similar domain movements occur in LRRK2 and CtRoco, and that the GTPγS-induced conformational changes that we observe are thus likely also relevant to LRRK2.

The second prominent conformational change that occurs upon GTPγS binding is the movement of the LRR domain away from the Roc and COR domains. We hypothesize that also this conformational change is initially triggered by changes in the Switch 2 region upon GTP binding. In the nucleotide-free state, the backside of Switch 2 interacts with the LRR domain and the LRR-Roc linker via residues Q527, F528 and R532 (Deyaert et al., 2019). Rearrangement of Switch 2 upon nucleotide binding would disrupt these interactions. A key element for these conformational

changes is the linker region between the LRR and Roc domains, with the α_0-helix that immediately precedes the Roc domain playing a central role. While the α_0-helix is buried in between the LRR, Roc and CORA domain in the dimer, it loses all interactions with these domains in the GTPγS-bound monomer, and acts as the swivel point for the rotational movement of the LRR domain **(Figure 2)**. The conformational changes in the LRR domain upon nucleotide-induced activation of CtRoco are reminiscent to the observed changes in this domain upon activation of LRRK2 by Rab29 (Zhu et al., 2022). Indeed, in the kinase-inactive state of LRRK2, the LRR domain wraps around the kinase domain hence obstructing the entry of bulky substrates in the ATP pocket (Myasnikov et al., 2021). However, upon activation by Rab29 the N-terminal domains, including the LRR, become disordered liberating the access to the active site of the kinase domain. Superposition of the inactive CtRoco dimer with inactive LRRK2, shows a very similar position of their LRR domains and α_0-helices, suggesting also comparable conformational changes upon activation (**Figure 6**). In agreement with these findings, recent molecular dynamics simulations proposed a key role for the LRR-Roc linker in the activation of LRRK2 (Weng et al., 2023). Moreover, a R1325Q variant in the α_0-helix of LRRK2 was recently identified as a kinase-activating PD mutation (Kalogeropulou et al., 2022). In LRRK2, R1325 interacts with F1284, N1286, and N1305 located at the C-terminus of the LRR domain and with P1524 located in the linker between Roc and CORA, and one could imagine that the R1325Q mutation would weaken the interaction between the LRR and Roc-COR domains and activate the kinase. The above mechanisms thus suggest a strong coupling between CtRoco monomerization and the conformational changes within each protomer. Such a link between monomerization and activation was recently also suggested in LRRK2, by the finding that mutations in the CORB:CORB dimer interface (R1731L / R1731D) enhance LRRK2 kinase activity (Snead et al., 2022).

Next to these insights in the nucleotide-mediated activation mechanism of Roco proteins, our structure also reveals how Nb_{Roco1} and Nb_{Roco2} can allosterically activate the GTPase activity of

CtRoco. The most prominent role in this regard seems to be for Nb_{Roco1}, which binds in the region of CtRoco that undergoes the largest conformational changes upon GTP-driven monomerization, consisting of the linker regions connecting the LRR to the Roc domain and the Roc to the CORA domain **(Figure 3)**. The extended conformation of the CtRoco monomer is further stabilized by the binding of Nb_{Roco2} in the curvature of the horseshoe-shaped LRR domain, which would sterically exclude the LRR conformation adopted in the compact CtRoco dimer. We also find that Nb_{Roco1} and Nb_{Roco2} cooperate in shifting the CtRoco dimer-monomer equilibrium toward the activated monomer, since binding of Nb_{Roco2} to nucleotide-free CtRoco allows the subsequent binding of Nb_{Roco1}. This again proves that the conformational changes occurring upon CtRoco activation are closely linked and act in a concerted manner. Correspondingly, the bi-valent/bi-paratopic $Nb_{R2\text{-}R1}$ construct shows an increased affinity towards CtRoco and a very strong stimulation of the GTPase activity of the slow CtRoco-L487A mutant, illustrating the power of the cooperative avidity effects enabled by such bivalent constructs. Considering that the conformational changes of the LRR domain, and the role of the LRR-Roc linker in this regard, are conserved features within the activation mechanisms of CtRoco and LRRK2, one could imagine that a similar mode-of-action could also be applicable to Nbs binding to LRRK2. Previously, we described Nbs that can allosterically inhibit or activate the kinase activity of human LRRK2, but the exact mechanism underlying this activity is still elusive, and is it unclear whether these Nbs use similar mechanisms to the GTPase-activating Nbs described here (Singh et al., 2022). Such a set of Nbs that either modify the GTPase or kinase activity of LRRK2 would form exquisite tools to aid in unraveling the link between both catalytic activities, as well as the role of the GTPase in LRRK2 pathology.

In conclusion, our current study provides important new structural insights in the mechanism of activation of Roco proteins with relevance for LRRK2, suggests new avenues for allosteric modulation of Roco activity, and underscores remaining open questions with regard to the communication between GTPase and kinase activities in LRRK2.

Methods

Cloning of the bi-valent Nanobody construct

To generate the bi-valent Nb_{R2-R1}, a gene construct was designed that fuses the Nb_{Roco2} to the Nb_{Roco1} open reading frame with the following linker sequence:

5'-GGCGGCGGCGGCAGCGGCGGCGGCGGCAGCGGCGGCGGCGGCAGC-3'.

The gene was synthesized and subcloned by GenScript Biotech (Nederlands) in the pHEN29 vector which adds the Sortase-recognition sequence LPETG at the C-terminus, allowing for Sortase A-mediated labeling. The plasmid was initially transformed in *Escherichia coli* DH5α cells and subsequently in WK6 cells for protein expression.

Protein expression and purification

CtRoco, CtRoco-L487A, Nb_{Roco1} and Nb_{Roco2} were expressed and purified as previously described (Leemans et al., 2020). In brief, CtRoco and CtRoco-L487A were produced with an N-terminal His-tag from the pProEX plasmid in an *E. coli* BL21(DE3) strain. For purification, the protein was first subjected to a Ni^{2+}-NTA immobilized metal affinity chromatography step, using a His-trap FF column. After elution, the protein was dialyzed against 20 mM HEPES/NaOH pH 7.5, 150 mM NaCl, 5% glycerol, 1 mM DTT, and 1 mM EDTA was added to the protein to disrupt Mg^{2+} and nucleotide binding. As a second purification step a size exclusion chromatography on a Superdex 200 column (GE Healthcare) was performed, using the same buffer. After gel filtration 5 mM $MgCl_2$ was added to the protein sample and analytical reversed-phase chromatography was used to confirm the complete removal of nucleotides, as described previously (Deyaert, Wauters, et al., 2017). Samples were concentrated and flash frozen until use.

Nb_{Roco1} and Nb_{Roco2} and Nb_{R2-R1} were produced in *E. coli* WK6 cells with either a C-terminal His-tag from a pMESy4 vector (for structural studies), or with a C-terminal Sortase-His-tag from a pHEN29

vector (for fluorescent labeling). After an osmotic shock to obtain the periplasmic fraction, an affinity purification step on Ni^{2+}-NTA sepharose was performed followed by size exclusion chromatography on a Superdex 75 column equilibrated with the same buffer as used for the CtRoco protein.

Sample preparation and cryo-EM data acquisition

CtRoco was loaded with GTPγS by incubation with 0.5 mM of the nucleotide. Subsequently, the GTPγS-loaded protein was incubated with either Nb_{Roco1} alone (CtRoco-Nb_{Roco1}) or with Nb_{Roco1} and Nb_{Roco2} (CtRoco-Nb_{Roco1}-Nb_{Roco2}), using a 2x molar excess of the Nbs. A size exclusion chromatography was performed using a Superdex200 column to separate the Nb excess from the complex, the sample was immediately supplemented again with an excess of GTPγS, and the concentration of the sample was adjusted to 0.08 mg/ml. Quantifoil (2/1) 300-mesh copper holey grids were glow-discharged for 30 sec to 1 min, and 3 µl of the complex was loaded on the grid and blotted for 1 second using Whatman paper, before being frozen in liquid ethane on a Cryoplunge™3. Grids were stored in liquid nitrogen until use.

Single particle cryo-EM data were collected on a JEOL CryoARM300 transmission-electron microscope, operated at 300 kV and at a nominal magnification of 60,000 and corresponding pixel size of 0.76 Å. The microscope contained an omega energy filter with a slit width set to 20 eV. The images were recorded using a K3 detector (Gatan) operating in correlative-double sampling (CDS) mode. Micrographs were recorded as movies of 60 frames using SerialEM v3.0.8. A total of 11,718 movies were collected for the CtRoco-Nb_{Roco1} data set and 7,489 movies were collected for the CtRoco-Nb_{Roco1}-Nb_{Roco2} data set. Data-collection statistics are reported in **Table 1.**

Image processing

Data were processed on the fly using Relion 3.1 (Zivanov et al., 2018) including gain normalization, motion correction and calculation of dose-weighted averages with UCSF MotionCor2 (Zheng et al., 2017). Results were analyzed and curated in first instance using the in-house script BXEMALYZER (Shkumatov et al; in preparation). The motion corrected micrographs were imported into CryoSPARC v4.3 (Punjani et al., 2017) and CTF was calculated using Patch CTF.

For the CtRoco-Nb_{Roco1} data set, particle picking was first performed using manual picking followed by template picker (using initial 2D classes). After several rounds of 2D classification an ab initio reconstruction was obtained. Particles stacks from 2D classes that showed clear features of the full complex were selected for further processing, and together with the initial map imported into Relion 3.1. 3D auto-refine was performed in Relion, aligned particle stacks and models were imported back to CryoSPARC and particles reextracted with updated particle coordinates; this procedure improved the centering of the particles resulting in more classes displaying the full particle. A heterogeneous refinement with four classes, followed by homogeneous refinement of the best class based on density interpretability yielded a 8.3 Å resolution map reconstruction from 99,460 particles (**Figure 1–figure supplement 2)**.

For the CtRoco-Nb_{Roco1}-Nb_{Roco2} data set particle picking was first performed with Topaz (Bepler et al., 2019), after import of the micrographs to cryoSPARC, using the pre-trained model ResNet16 on a small set of 18 random images. Bad particles were removed by 2D classification and the rest were used to train a Topaz model, followed by picking using Topaz Extract on the full data set, which resulted in 716,919 particles extracted on a box size of 389 Å. After three rounds of 2D classification 371,956 particles were selected. Selected particles were used for multiple ab initio reconstruction using 6 classes followed by heterogeneous refinement of the 6 classes. These jobs yielded one class corresponding to the volume of CtRoco bound to both Nbs and two classes corresponding to good quality volumes centered on the LRR domain but with little density for the

other half of the molecule. The other three classes were also centered on the LRR domain but with overall bad quality. Homogeneous refinement of the class displaying a nearly full CtRoco protein bound to the two Nbs, followed by non-uniform refinement (Punjani et al., 2020), resulted in a 7.7 Å resolution map reconstruction from 48,333 particles. To obtain a focused map on the LRR half of the protein, the two classes centered on the LRR domain were merged, particles were reextracted on a smaller box size of 243 Å, and, after homogeneous and non-uniform refinements, a map was obtained where only the LRR domain bound to Nb_{Roco2} is visible with 3.6 Å resolution using 160,925 particles. To obtain a higher resolution map for the other half of the protein, spanning the Roc-COR and Nb_{Roco1}, a different approach was used: three 2D classes centered on the Roc-COR domains were selected and fed to a template picker job with the intention to pick this half of the particles only, and extracted on a box size of 243 Å. After extraction and three rounds of 2D classification, again only classes that were centered on the Roc-COR domains were selected for ab initio reconstruction using four classes followed by heterogeneous refinement. These yielded one good quality volume and the particles in this class were then subjected to non-uniform refinement, yielding a map representing the Roc-COR domains and the Nb_{Roco1}. The overall resolution of the map was estimated at 3.9 Å using 38,260 particles (**Figure 1–figure supplement 1**).

Model building and refinement

The focused maps containing either the LRR domain bound to Nb_{Roco2} or the Roc-COR domain bound to Nb_{Roco1} were improved by density modification with resolve_cryo_em (Terwilliger et al., 2020) in the PHENIX suit (version 1.20.1) (Adams et al., 2010), and used for model interpretation and refinement. Initial models of the individual CtRoco domains were taken from the nucleotide-free CtRoco structure (PDB: 6hlu). Nb models were generated using AlphaFold2 (Jumper et al., 2021). Initial rigid body fits were performed for each domain separately on UCSF ChimeraX 1.2 (Pettersen et al., 2021), followed by a flexible fitting in Coot 0.9.2 (Emsley et al., 2010) to fit the

secondary structure features into density. Manual building and inspection was also done in Coot, and real-space refinement was performed with the phenix.real_space_refine program in PHENIX applying Ramachandran plot restrains. Model-versus-data fit was assessed by curves of the Fourier shell correlation (FSC) as a function of resolution using the refined models and the two half-maps of each focused volume (**Figure 1–figure supplement 5**). Finally, the focused maps and models were fitted into the lower resolution map of the entire protein in UCSF ChimeraX to obtain an overall interpretation of CtRoco-Nb_{Roco1}-Nb_{Roco2}. Figures containing molecular structures and volumes were prepared with UCSF ChimeraX and PyMOL (The PyMol Molecular Graphic System, version 2.4 Schrödinger, LLC, https://pymol.org/2/). Maps shown in the figures were improved with either Resolve or EMReady (He et al., 2023).

Chemical crosslinking mass spectrometry

CX-MS was performed as previously described (Singh et al., 2022). Briefly, the CtRoco concentration was adjusted to 8 µM in storage buffer. GTPγS-bound CtRoco was crosslinked with DSSO at a molar ratio of 1:50 (protein: crosslinker). In addition, GTPγS-bound CtRoco was mixed with either Nb_{Roco1}, Nb_{Roco2} or both in a molar ratio 1:5 (CtRoco:Nb) before DSSO crosslinking (molar ratio 1:50). The reaction was carried on for 30 minutes at room temperature and stopped by adding 10 µL of 1 M Tris at pH 7.5. Proteins were precipitated by chloroform/methanol and subjected to tryptic proteolysis. The tryptic peptide solutions were cleaned up by C18-StageTips (Thermo Fisher) and the volume was reduced to approximately 10 µL in a SpeedVac. 40 µL Size Exclusion Chromatography (SEC) buffer (30% [vol/vol] acetonitrile, 0.1% TFA) was added to the desalted peptides. The entire volume of 50 µL was loaded onto the SEC column (Superdex Peptide column 3.2/300; Cytiva), which was mounted to an Äkta pure system (Cytiva) and equilibrated in SEC buffer. SEC was performed at a flow rate of 50 µL/min. The eluates were collected in 100 µL fractions. Vacuum-dried fractions (remaining volume of 2 µL to avoid complete dryness) containing

the crosslinked peptides, were re-dissolved in a total volume of 10 µL 0.5% TFA and analyzed individually on an Orbitrap Fusion mass spectrometer (Thermo Fisher) using the MS2_MS3 fragmentation method with the default settings (ver. 3.4, build 3072). MS1 scans were performed in the Orbitrap (FTMS, resolution = 60K) at an m/z range of 375-1500. MS2 was performed with CID (CE=25%) and spectra were acquired in the Orbitap (FTMS) at 30K resolution. The MS3 scans were performed with HCD (CE=30%) and spectra were acquired in the linear ion trap. Resulting Thermo Raw files were analyzed with the MS2_MS3 workflow provided by in Proteome Discoverer 2.5 (build 2.5.0.400) using XlinkX (version 2.5).

Fluorescence anisotropy titrations

The affinity of Nb_{Roco1}, Nb_{Roco2} and $Nb_{R2\text{-}R1}$ for CtRoco was determined using fluorescence anisotropy titrations, Nbs were labeled at their C-terminus with a FITC fluorophore using Sortase A-mediated labeling, as previously described (Leemans et al., 2020). Fluorescence anisotropy titrations with FITC-labeled Nbs and CtRoco were performed at 25°C using a Cary Eclipse spectrofluorometer (Agilent) equipped with polarizers and temperature control, at an excitation wavelength of 493 nm and emission wavelength of 516 nm. 50 nM FITC-labeled Nb was titrated with increasing amounts of CtRoco. The anisotropy signal was measured after a 2 min incubation period for each titration. All experiments were performed in triplicate. To obtain Kd values (± standard error), the data were fitted using the quadratic binding equation in GraphPad Prism 7.

Single turn-over kinetics

GTP hydrolysis rates were calculated under single turn-over conditions. 5 µM of CtRoco-L487A was incubated with 5 µM of GTP in the presence of 100 µM of the Nb of interest at 25 °C. Samples were taken at different time points ranging from 0 to 180 min and the reaction was stopped by incubation at 95°C for 3 min. Samples were mixed with the same volume of HPLC buffer and 50 µl

was injected on a reversed-phase C18 column (Phenomenex, Jupiter 5 mm) attached to an Alliance e2695 HPLC (Waters) using 100 mM KH_2PO_4 pH 6.4, 10 mM tetrabutylammonium bromide, 7.5% acetonitrile as the mobile phase. The 254 nm absorption peaks of GDP were converted to concentrations by using a standard curve, and GDP concentrations were plotted in function of time. All experiments were performed in triplicate and data were fitted on single-exponential equation using GraphPad Prism 7.

Author Contributions

C.G. performed most of the experimental work and analyzed data; G.G. performed the XL-MS experiment; M.F. supervised cryo-EM data collection and assisted in data analysis; C.J.G. analyzed and interpreted the XL-MS experiment and contributed to the writing of the manuscript; W.V. conceived the study and analyzed and interpreted data; C.G. and W.V. wrote the manuscript with the help and input of all other authors.

Acknowledgements

We would like to thank Siemen Claeys for excellent technical support, Jonathan Mitano for his assistance in some of the experiments, and all members of the Versées lab for comments and discussions. We also thank Dirk Reiter from the BECM cryo-EM facility for EM computational support. The authors wish to thank the staff of the Core Facility for Medical Proteomics (Tübingen) for technical assistance. This work was supported by grants from the Research Foundation Flanders [G005219N, G003322N] and a Strategic Research Program Financing from the VUB [SRP50].

Data availability

Cryo-EM Density maps and structure coordinates have been deposited in the Electron Microscopy Data Bank (EMDB) and the Protein Data Bank (PDB), with accession codes EMD-18884 and PDB

8R4B for the composite map and structure of CtRoco-Nb_{Roco1}-Nb_{Roco2}, EMD-18885 and PDB 8R4C for the LRR-Nb_{Roco2} focused map and structure, EMD-1886 and PDB 8R4D for the Roc-COR-Nb_{Roco1} focused map and structure, EMD-18882 for the low resolution full CtRoco-Nb_{Roco1}-Nb_{Roco2} map, and EMD-18879 for the CtRoco-Nb_{Roco1} map.

The XL-MS data have been deposited to the ProteomeXchange Consortium via the PRIDE (Perez-Riverol et al., 2019) partner repository with the dataset identifier PXD046634 and 10.6019/PXD046634.

References

Adams, P. D., Afonine, P. V, Bunkóczi, G., Chen, V. B., Davis, I. W., Echols, N., Headd, J. J., Hung, L.-W., Kapral, G. J., Grosse-Kunstleve, R. W., McCoy, A. J., Moriarty, N. W., Oeffner, R., Read, R. J., Richardson, D. C., Richardson, J. S., Terwilliger, T. C., & Zwart, P. H. (2010). PHENIX: a comprehensive Python-based system for macromolecular structure solution. *Acta Crystallographica. Section D, Biological Crystallography*, *66*, 213–221. https://doi.org/10.1107/S0907444909052925

Bepler, T., Morin, A., Rapp, M., Brasch, J., Shapiro, L., Noble, A. J., & Berger, B. (2019). Positive-unlabeled convolutional neural networks for particle picking in cryo-electron micrographs. *Nature Methods*, *16*(11), 1153–1160. https://doi.org/10.1038/s41592-019-0575-8

Bosgraaf, L., & Van Haastert, P. J. M. (2003). Roc, a Ras/GTPase domain in complex proteins. *Biochimica et Biophysica Acta*, *1643*(1–3), 5–10. https://doi.org/10.1016/j.bbamcr.2003.08.008

Cogo, S., Ho, F. Y., Tosoni, E., Tomkins, J. E., Tessari, I., Iannotta, L., Montine, T. J., Manzoni, C., Lewis, P. A., Bubacco, L., Chartier Harlin, M. C., Taymans, J. M., Kortholt, A., Nichols, J., Cendron, L., Civiero, L., & Greggio, E. (2022). The Roc domain of LRRK2 as a hub for protein-protein interactions: a focus on PAK6 and its impact on RAB phosphorylation. *Brain Research*, *1778*, 147781. https://doi.org/10.1016/J.BRAINRES.2022.147781

Deniston, C. K., Salogiannis, J., Mathea, S., Snead, D. M., Lahiri, I., Matyszewski, M., Donosa, O., Watanabe, R., Böhning, J., Shiau, A. K., Knapp, S., Villa, E., Reck-Peterson, S. L., & Leschziner, A. E. (2020). Structure of LRRK2 in Parkinson's disease and model for microtubule interaction. *Nature*, *588*(7837), 344–349. https://doi.org/10.1038/s41586-020-2673-2

Deyaert, E., Kortholt, A., & Versées, W. (2017). The LRR-Roc-COR module of the Chlorobium tepidum Roco protein: crystallization and X-ray crystallographic analysis. *Acta Crystallographica. Section F, Structural Biology Communications*, *73*(Pt 9), 520–524. https://doi.org/10.1107/S2053230X17011955

Deyaert, E., Leemans, M., Singh, R. K., Gallardo, R., Steyaert, J., Kortholt, A., Lauer, J., & Versées, W. (2019). Structure and nucleotide-induced conformational dynamics of the Chlorobium tepidum Roco protein. *The Biochemical Journal*, *476*(1), 51–66. https://doi.org/10.1042/BCJ20180803

Deyaert, E., Wauters, L., Guaitoli, G., Konijnenberg, A., Leemans, M., Terheyden, S., Petrovic, A., Gallardo, R., Nederveen-Schippers, L. M., Athanasopoulos, P. S., Pots, H., Van Haastert, P. J. M., Sobott, F., Gloeckner, C. J., Efremov, R., Kortholt, A., & Versées, W. (2017). A homologue of the Parkinson's disease-associated protein LRRK2 undergoes a monomer-dimer transition during GTP turnover. *Nature Communications*, *8*(1), 1–12. https://doi.org/10.1038/s41467-017-01103-4

Di Maio, R., Hoffman, E. K., Rocha, E. M., Keeney, M. T., Sanders, L. H., De Miranda, B. R., Zharikov, A., Van Laar, A., Stepan, A. F., Lanz, T. A., Kofler, J. K., Burton, E. A., Alessi, D. R., Hastings, T. G., & Greenamyre, J. T. (2018). LRRK2 activation in idiopathic Parkinson's disease. *Science Translational Medicine*, *10*(451). https://doi.org/10.1126/scitranslmed.aar5429

Emsley, P., Lohkamp, B., Scott, W. G., & Cowtan, K. (2010). Features and development of Coot. *Acta Crystallographica Section D: Biological Crystallography*, *66*, 486–501. https://doi.org/10.1107/S0907444910007493

Erzberger, J. P., Stengel, F., Pellarin, R., Zhang, S., Schaefer, T., Aylett, C. H. S., Cimermančič, P., Boehringer, D., Sali, A., Aebersold, R., & Ban, N. (2014). Molecular architecture of the 40S·eIF1·eIF3 translation initiation complex. *Cell*, *158*(5), 1123–1135. https://doi.org/10.1016/j.cell.2014.07.044

Gilks, W. P., Abou-Sleiman, P. M., Gandhi, S., Jain, S., Singleton, A., Lees, A. J., Shaw, K., Bhatia, K. P., Bonifati, V., Quinn, N. P., Lynch, J., Healy, D. G., Holton, J. L., Revesz, T., & Wood, N. W. (2005). A common LRRK2 mutation in idiopathic Parkinson's disease. *The Lancet*, *365*(9457), 415–416. https://doi.org/10.1016/S0140-6736(05)17830-1

Gilsbach, B. K., Ho, F. Y., Riebenbauer, B., Zhang, X., & Guaitoli, G. (2023). Intramolecular feedback regulation of the LRRK2 Roc G domain by a LRRK2 kinase dependent mechanism. *BioRxiv*. https://doi.org/10.1101/2023.07.31.549909

Gotthardt, K., Weyand, M., Kortholt, A., Van Haastert, P. J. M., & Wittinghofer, A. (2008). Structure of the Roc-COR domain tandem of C. tepidum, a prokaryotic homologue of the human LRRK2 Parkinson kinase. *The EMBO Journal*, *27*(16), 2239–2249. https://doi.org/10.1038/emboj.2008.150

Guaitoli, G., Raimondi, F., Gilsbach, B. K., Gómez-Llorente, Y., Deyaert, E., Renzi, F., Li, X., Schaffner, A., Jagtap, P. K. A., Boldt, K., von Zweydorf, F., Gotthardt, K., Lorimer, D. D., Yue, Z., Burgin, A., Janjic, N., Sattler, M., Versées, W., Ueffing, M., … Gloeckner, C. J. (2016). Structural model of the dimeric Parkinson's protein LRRK2 reveals a compact architecture involving distant interdomain contacts. *Proceedings of the National Academy of Sciences of the United States of America*, *113*(30), E4357-66. https://doi.org/10.1073/pnas.1523708113

He, J., Li, T., & Huang, S. Y. (2023). Improvement of cryo-EM maps by simultaneous local and non-local deep learning. *Nature Communications 2023 14:1*, *14*(1), 1–16. https://doi.org/10.1038/s41467-023-39031-1

Helton, L. G., Soliman, A., von Zweydorf, F., Kentros, M., Manschwetus, J. T., Hall, S., Gilsbach, B., Ho, F. Y., Athanasopoulos, P. S., Singh, R. K., LeClair, T. J., Versées, W., Raimondi, F., Herberg, F. W., Gloeckner, C. J., Rideout, H., Kortholt, A., & Kennedy, E. J. (2021). Allosteric Inhibition of Parkinson's-Linked LRRK2 by Constrained Peptides. *ACS Chemical Biology*, *16*(11), 2326–2338. https://doi.org/10.1021/acschembio.1c00487

Hui, K. Y., Fernandez-Hernandez, H., Hu, J., Schaffner, A., Pankratz, N., Hsu, N.-Y., Chuang, L.-S., Carmi, S., Villaverde, N., Li, X., Rivas, M., Levine, A. P., Bao, X., Labrias, P. R., Haritunians, T., Ruane, D.,

Gettler, K., Chen, E., Li, D., … Peter, I. (2018). Functional variants in the LRRK2 gene confer shared effects on risk for Crohn's disease and Parkinson's disease. *Science Translational Medicine*, *10*(423). https://doi.org/10.1126/scitranslmed.aai7795

Jagtap, S., Potdar, C., Yadav, R., Pal, P. K., & Datta, I. (2022). Dopaminergic Neurons Differentiated from LRRK2 I1371V-Induced Pluripotent Stem Cells Display a Lower Yield, α-Synuclein Pathology, and Functional Impairment. *ACS Chemical Neuroscience*, *13*(17), 2632–2645. https://doi.org/10.1021/acschemneuro.2c00297

Jumper, J., Evans, R., Pritzel, A., Green, T., Figurnov, M., Ronneberger, O., Tunyasuvunakool, K., Bates, R., Žídek, A., Potapenko, A., Bridgland, A., Meyer, C., Kohl, S. A. A., Ballard, A. J., Cowie, A., Romera-Paredes, B., Nikolov, S., Jain, R., Adler, J., … Hassabis, D. (2021). Highly accurate protein structure prediction with AlphaFold. *Nature 2021 596:7873*, *596*(7873), 583–589. https://doi.org/10.1038/s41586-021-03819-2

Kalogeropulou, A. F., Purlyte, E., Tonelli, F., Lange, S. M., Wightman, M., Prescott, A. R., Padmanabhan, S., Sammler, E., & Alessi, D. R. (2022). Impact of 100 LRRK2 variants linked to Parkinson's disease on kinase activity and microtubule binding. *The Biochemical Journal*, *479*(17), 1759–1783. https://doi.org/10.1042/BCJ20220161

Kao, A., Chiu, C., Vellucci, D., Yang, Y., Patel, V. R., Guan, S., Randall, A., Baldi, P., Rychnovsky, S. D., & Huang, L. (2011). Development of a novel cross-linking strategy for fast and accurate identification of cross-linked peptides of protein complexes. *Molecular & Cellular Proteomics : MCP*, *10*(1), M110.002212. https://doi.org/10.1074/mcp.M110.002212

Leemans, M., Galicia, C., Deyaert, E., Daems, E., Krause, L., Paesmans, J., Pardon, E., Steyaert, J., Kortholt, A., Sobott, F., Klostermeier, D., & Versées, W. (2020). Allosteric modulation of the GTPase activity of a bacterial LRRK2 homolog by conformation-specific Nanobodies. *The Biochemical Journal*, *477*(7), 1203–1218. https://doi.org/10.1042/BCJ20190843

Lewis, P. A., Greggio, E., Beilina, A., Jain, S., Baker, A., & Cookson, M. R. (2007). The R1441C mutation of LRRK2 disrupts GTP hydrolysis. *Biochemical and Biophysical Research Communications*, *357*(3), 668–671. https://doi.org/10.1016/j.bbrc.2007.04.006

Liu, Z., Bryant, N., Kumaran, R., Beilina, A., Abeliovich, A., Cookson, M. R., & West, A. B. (2018). LRRK2 phosphorylates membrane-bound Rabs and is activated by GTP-bound Rab7L1 to promote recruitment to the trans-Golgi network. *Human Molecular Genetics*, *27*(2), 385–395. https://doi.org/10.1093/hmg/ddx410

Myasnikov, A., Zhu, H., Hixson, P., Xie, B., Yu, K., Pitre, A., Peng, J., & Sun, J. (2021). Structural analysis of the full-length human LRRK2. *Cell*, *184*(13), 3519-3527.e10. https://doi.org/10.1016/j.cell.2021.05.004

Paisán-Ruíz, C., Jain, S., Evans, E. W., Gilks, W. P., Simón, J., van der Brug, M., López de Munain, A., Aparicio, S., Gil, A. M., Khan, N., Johnson, J., Martinez, J. R., Nicholl, D., Martí Carrera, I., Pena, A. S., de Silva, R., Lees, A., Martí-Massó, J. F., Pérez-Tur, J., … Singleton, A. B. (2004). Cloning of the gene containing mutations that cause PARK8-linked Parkinson's disease. *Neuron*, *44*(4), 595–600. https://doi.org/10.1016/j.neuron.2004.10.023

Paisán-Ruíz, C., Lang, A. E., Kawarai, T., Sato, C., Salehi-Rad, S., Fisman, G. K., Al-Khairallah, T., St George-Hyslop, P., Singleton, A., & Rogaeva, E. (2005). LRRK2 gene in Parkinson disease: mutation

analysis and case control association study. *Neurology*, *65*(5), 696–700. https://doi.org/10.1212/01.wnl.0000167552.79769.b3

Park, Y., Liao, J., & Hoang, Q. Q. (2022). Roc, the G-domain of the Parkinson's disease-associated protein LRRK2. *Trends in Biochemical Sciences*, *47*(12), 1038–1047. https://doi.org/10.1016/j.tibs.2022.06.009

Pathak, P., Alexander, K. K., Helton, L. G., Kentros, M., LeClair, T. J., Zhang, X., Ho, F. Y., Moore, T. T., Hall, S., Guaitoli, G., Gloeckner, C. J., Kortholt, A., Rideout, H., & Kennedy, E. J. (2023). Doubly Constrained C-terminal of Roc (COR) Domain-Derived Peptides Inhibit Leucine-Rich Repeat Kinase 2 (LRRK2) Dimerization. *ACS Chemical Neuroscience*, *14*(11), 1971–1980. https://doi.org/10.1021/acschemneuro.3c00259

Perez-Riverol, Y., Csordas, A., Bai, J., Bernal-Llinares, M., Hewapathirana, S., Kundu, D. J., Inuganti, A., Griss, J., Mayer, G., Eisenacher, M., Pérez, E., Uszkoreit, J., Pfeuffer, J., Sachsenberg, T., Yilmaz, S., Tiwary, S., Cox, J., Audain, E., Walzer, M., … Vizcaíno, J. A. (2019). The PRIDE database and related tools and resources in 2019: improving support for quantification data. *Nucleic Acids Research*, *47*(D1), D442–D450. https://doi.org/10.1093/nar/gky1106

Pettersen, E. F., Goddard, T. D., Huang, C. C., Meng, E. C., Couch, G. S., Croll, T. I., Morris, J. H., & Ferrin, T. E. (2021). UCSF ChimeraX: Structure visualization for researchers, educators, and developers. *Protein Science*, *30*(1), 70–82. https://doi.org/10.1002/PRO.3943

Punjani, A., Zhang, H., & Fleet, D. J. (2020). Non-uniform refinement: adaptive regularization improves single-particle cryo-EM reconstruction. *Nature Methods*, *17*(12), 1214–1221. https://doi.org/10.1038/s41592-020-00990-8

Singh, R. K., Soliman, A., Guaitoli, G., Störmer, E., von Zweydorf, F., Dal Maso, T., Oun, A., Van Rillaer, L., Schmidt, S. H., Chatterjee, D., David, J. A., Pardon, E., Schwartz, T. U., Knapp, S., Kennedy, E. J., Steyaert, J., Herberg, F. W., Kortholt, A., Gloeckner, C. J., & Versées, W. (2022). Nanobodies as allosteric modulators of Parkinson's disease-associated LRRK2. *Proceedings of the National Academy of Sciences of the United States of America*, *119*(9). https://doi.org/10.1073/pnas.2112712119

Snead, D. M., Matyszewski, M., Dickey, A. M., Lin, Y. X., Leschziner, A. E., & Reck-Peterson, S. L. (2022). Structural basis for Parkinson's disease-linked LRRK2's binding to microtubules. *Nature Structural & Molecular Biology*, *29*(12), 1196–1207. https://doi.org/10.1038/s41594-022-00863-y

Steger, M., Diez, F., Dhekne, H. S., Lis, P., Nirujogi, R. S., Karayel, O., Tonelli, F., Martinez, T. N., Lorentzen, E., Pfeffer, S. R., Alessi, D. R., & Mann, M. (2017). Systematic proteomic analysis of LRRK2-mediated Rab GTPase phosphorylation establishes a connection to ciliogenesis. *ELife*, *6*. https://doi.org/10.7554/eLife.31012

Steger, M., Tonelli, F., Ito, G., Davies, P., Trost, M., Vetter, M., Wachter, S., Lorentzen, E., Duddy, G., Wilson, S., Baptista, M. A., Fiske, B. K., Fell, M. J., Morrow, J. A., Reith, A. D., Alessi, D. R., & Mann, M. (2016). Phosphoproteomics reveals that Parkinson's disease kinase LRRK2 regulates a subset of Rab GTPases. *ELife*, *5*. https://doi.org/10.7554/eLife.12813

Störmer, E., Weng, J.-H., Wu, J., Bertinetti, D., Kaila Sharma, P., Ma, W., Herberg, F. W., & Taylor, S. S. (2023). Capturing the domain crosstalk in full length LRRK2 and LRRK2RCKW. *Biochemical Journal*, *480*(11), 815–833. https://doi.org/10.1042/BCJ20230126

Terwilliger, T. C., Ludtke, S. J., Read, R. J., Adams, P. D., & Afonine, P. V. (2020). Improvement of cryo-EM maps by density modification. *Nature Methods*, *17*(9), 923–927. https://doi.org/10.1038/s41592-020-0914-9

Uchański, T., Pardon, E., & Steyaert, J. (2020). Nanobodies to study protein conformational states. In *Current Opinion in Structural Biology* (Vol. 60, pp. 117–123). Elsevier Ltd. https://doi.org/10.1016/j.sbi.2020.01.003

Wauters, L., Terheyden, S., Gilsbach, B. K., Leemans, M., Athanasopoulos, P. S., Guaitoli, G., Wittinghofer, A., Gloeckner, C. J., Versées, W., & Kortholt, A. (2018). Biochemical and kinetic properties of the complex Roco G-protein cycle. *Biological Chemistry*, *399*(12), 1447–1456. https://doi.org/10.1515/hsz-2018-0227

Wauters, L., Versées, W., & Kortholt, A. (2019). Roco Proteins: GTPases with a Baroque Structure and Mechanism. *International Journal of Molecular Sciences*, *20*(1). https://doi.org/10.3390/ijms20010147

Weng, J.-H., Trilling, C. R., Kaila Sharma, P., Störmer, E., Wu, J., Herberg, F. W., & Taylor, S. S. (2023). Novel LRR-ROC Motif That Links the N- and C-terminal Domains in LRRK2 Undergoes an Order-Disorder Transition Upon Activation. *Journal of Molecular Biology*, *435*(12), 167999. https://doi.org/10.1016/j.jmb.2023.167999

West, A. B., Moore, D. J., Biskup, S., Bugayenko, A., Smith, W. W., Ross, C. A., Dawson, V. L., & Dawson, T. M. (2005). Parkinson's disease-associated mutations in leucine-rich repeat kinase 2 augment kinase activity. *Proceedings of the National Academy of Sciences of the United States of America*, *102*(46), 16842–16847. https://doi.org/10.1073/pnas.0507360102

Zheng, S. Q., Palovcak, E., Armache, J.-P., Verba, K. A., Cheng, Y., & Agard, D. A. (2017). MotionCor2: anisotropic correction of beam-induced motion for improved cryo-electron microscopy. *Nature Methods*, *14*(4), 331–332. https://doi.org/10.1038/nmeth.4193

Zhu, H., Tonelli, F., Alessi, D. R., & Sun, J. (2022). Structural basis of human LRRK2 membrane recruitment and activation. *BioRxiv*. https://doi.org/10.1101/2022.04.26.489605

Zimprich, A., Biskup, S., Leitner, P., Lichtner, P., Farrer, M., Lincoln, S., Kachergus, J., Hulihan, M., Uitti, R. J., Calne, D. B., Stoessl, A. J., Pfeiffer, R. F., Patenge, N., Carbajal, I. C., Vieregge, P., Asmus, F., Müller-Myhsok, B., Dickson, D. W., Meitinger, T., … Gasser, T. (2004). Mutations in LRRK2 cause autosomal-dominant parkinsonism with pleomorphic pathology. *Neuron*, *44*(4), 601–607. https://doi.org/10.1016/j.neuron.2004.11.005

Zivanov, J., Nakane, T., Forsberg, B. O., Kimanius, D., Hagen, W. J. H., Lindahl, E., & Scheres, S. H. W. (2018). New tools for automated high-resolution cryo-EM structure determination in RELION-3. *ELife*, *7*, e42166. https://doi.org/10.7554/eLife.42166

Table 1. Cryo-EM data collection, refinement and validation statistics

	CtRoco-Nb$_{Roco1}$-Nb$_{Roco2}$	**CtRoco-Nb$_{Roco1}$-Nb$_{Roco2}$ (LRR focused)**	**CtRoco-Nb$_{Roco1}$-Nb$_{Roco2}$ (Roc-COR focused)**	**CtRoco-Nb$_{Roco1}$**
Data collection				
Microscope	CryoARM300			CryoARM300
Voltage (keV)	300			300
Electron exposure (e^-/Å^2)	63			63
Energy filter slit width	20 *eV*			20 *eV*
Detector	Gatan K3			Gatan K3
Magnification	x 60,000			x 60,000
Defocus range (μm)	1 – 3			1 – 3
Pixel size (Å/pix)	0.755			0.766
Number of movies	7,489			11,718
Symmetry	C1			C1
Final particles	48,333	160,925	38,260	99,460
Map mean resolution (Å)	7.7	3.6	3.9	8.3
Model refinement				
Atoms		4038	3573	
Bonds (RMSD)				
Bond length (Å)		0.004	0.003	
Bond angles (°)		0.749	0.647	
Validation				
Clash score		13.09	12.94	
Rotamer outliers (%)		0.7	0.3	
Ramachandran plot				
Favored (%)		88.57	89.78	
Allowed (%)		11.25	9.57	
Outlier (%)		0.18	0.65	

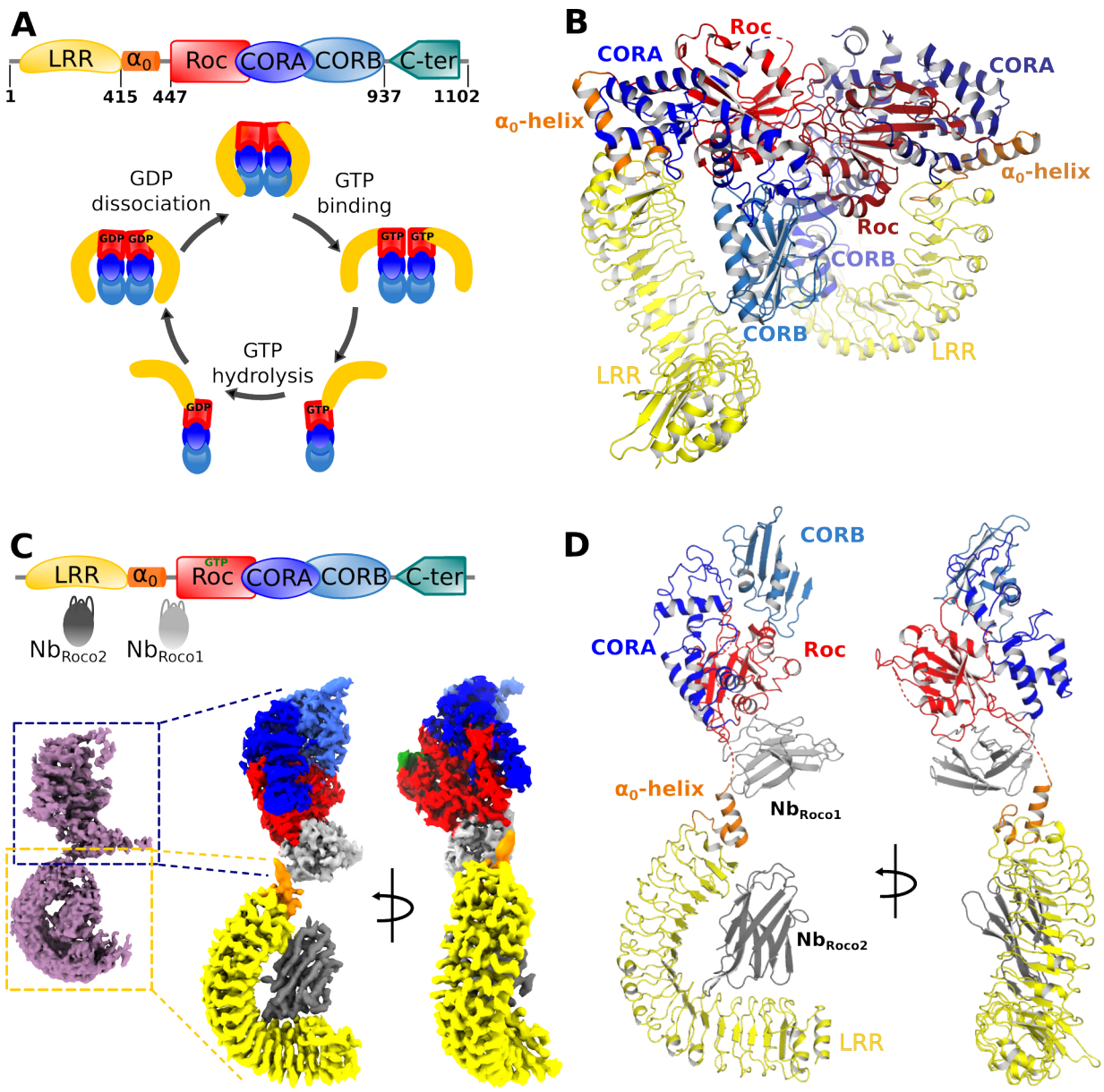

Figure 1. Nucleotide-induced conformational changes in CtRoco. **(A)** Schematic representation of the domain arrangement of CtRoco (*top*), and its anticipated conformational cycle linked to GTP binding and hydrolysis (*bottom*) (Deyaert, Wauters, et al., 2017). **(B)** The previously published crystal structure of nucleotide-free CtRoco showing the protein as a compact homodimer, where the LRR domains fold back on the Roc-COR domains (PDB: 6hlu) (Deyaert et al., 2019). (**C**) Nb_{Roco1} and Nb_{Roco2} specifically bind to the CtRoco monomer in its "GTP state" (*top*) (Leemans et al., 2020). The cryo-EM map of GTPγS-bound full-length CtRoco in complex with Nb_{Roco1} and Nb_{Roco2} at 7.7 Å resolution shows an elongated monomeric arrangement (*bottom-left*). A composite map, obtained by superposing the individual cryo-EM maps focused on the C-terminal (3.9 Å) and N-terminal (3.6 Å) part of the protein, was generated (*bottom-right*). This map is colored according to the corresponding domains and Nbs. (**D**) Final model of CtRoco-Nb_{Roco1}-Nb_{Roco2} based on the maps shown in (C).

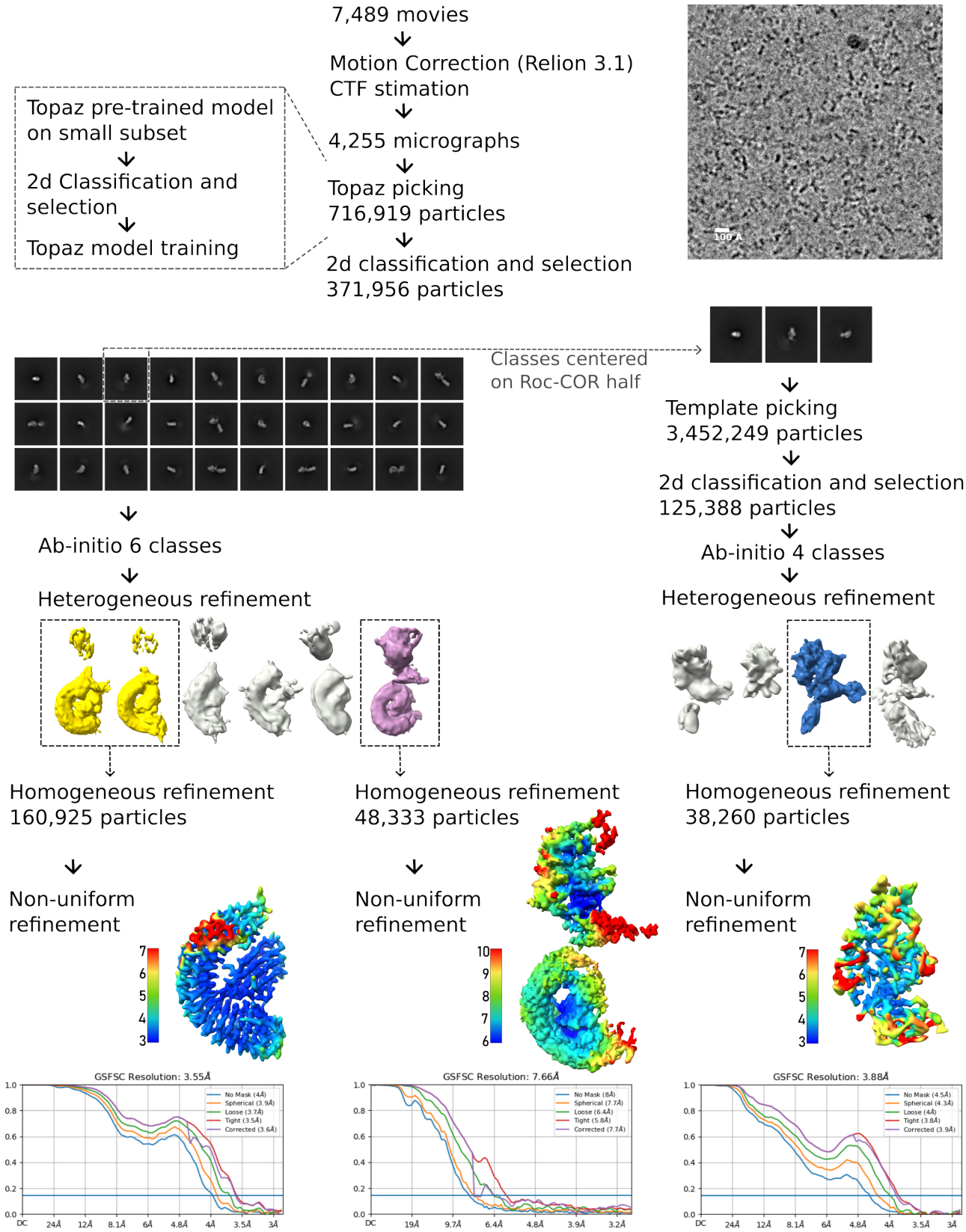

Figure1 - supplement 1. Cryo-electron microscopy (Cryo-EM) workflow to obtain the maps corresponding to CtRoco-Nb$_{Roco1}$-Nb$_{Roco2}$. Flow chart of the cryo-EM data processing, including 2D and 3D classifications, focused map strategies and density map reconstructions. Local resolution maps, FSC curves, and cryo-EM density maps are also shown. Unless otherwise stated, all analyses were performed using cryoSPARC v3.3. Details are provided in the Methods section.

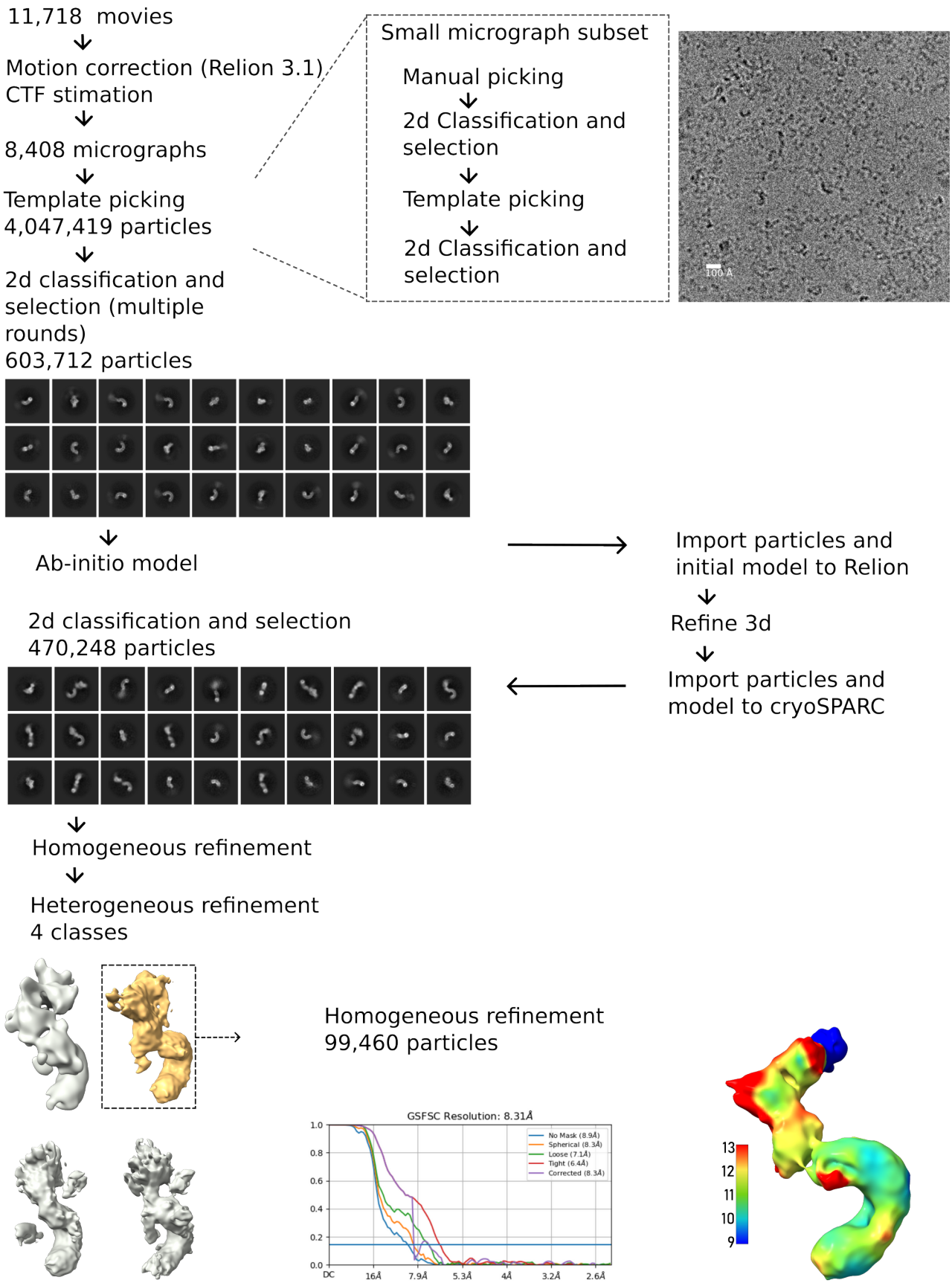

Figure1 - supplement 2. Cryo-electron microscopy (Cryo-EM) workflow to obtain the map corresponding to CtRoco-Nb$_{Roco1}$. Flow chart of the cryo-EM data processing, including 2D and 3D classifications and density map reconstructions. Local resolution map, FSC curve, and cryo-EM density map

are also shown. Unless otherwise stated, all analyses were performed using cryoSPARC v3.3. Details are provided in the Methods section.

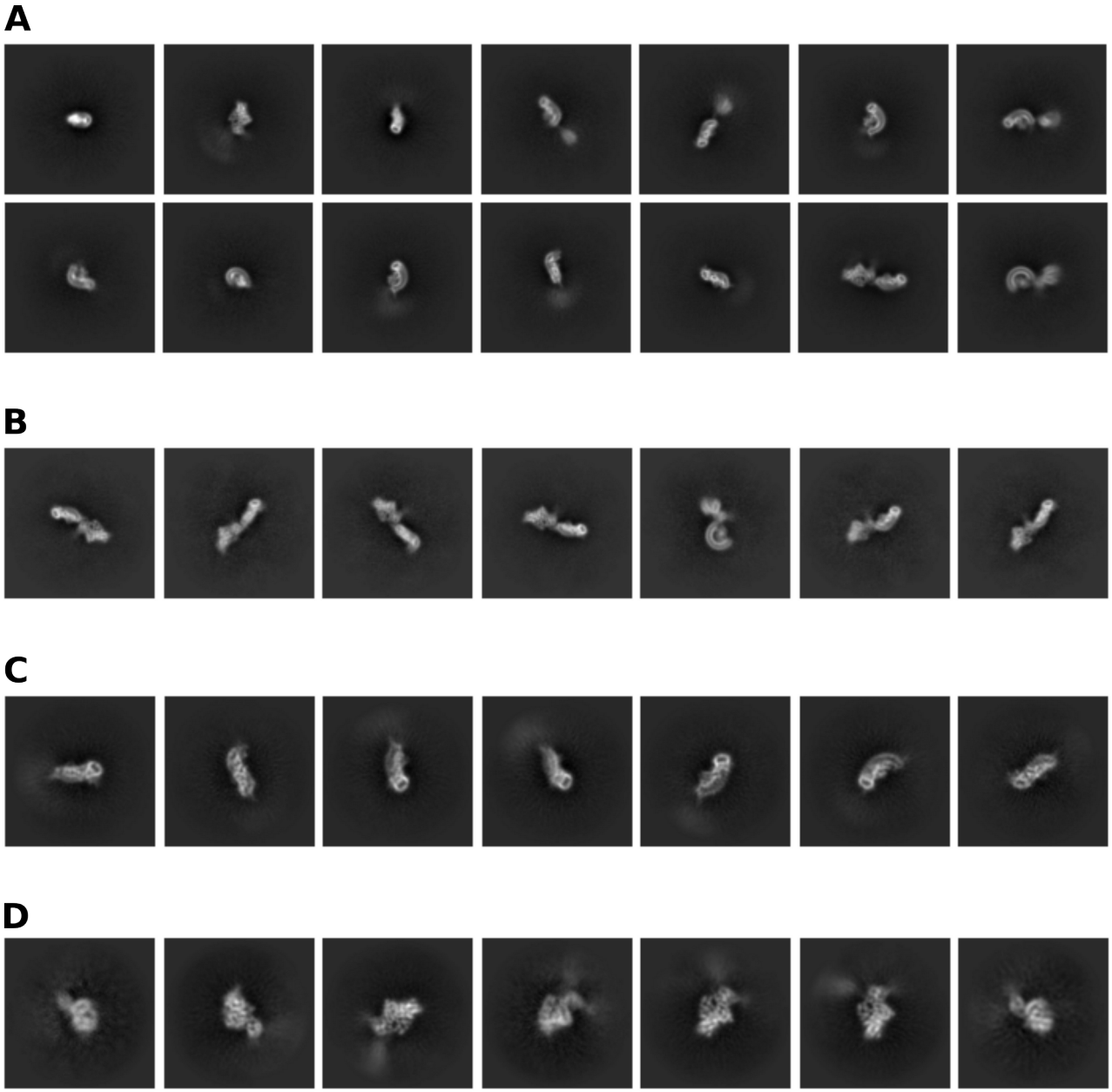

Figure 1 - supplement 3. 2D classification of CtRoco-Nb$_{Roco1}$-Nb$_{Roco2}$ (representative classes). (A) 2D classes from particles extracted in a box size of 384 Å. Only some of these classes display the full particle, most are centered on one half of the protein showing blurred density for the rest of the particle. **(B)** Selected classes displaying the pull particle. **(C)** 2D classes from particles selected for a focused map centered on the LRR domain, extracted in a box size of 243 Å. Blurred density for the rest of the particle is also visible. **(D)** 2D classes from particles selected for a focused map centered on the Roc-COR domains, extracted in a box size of 243 Å. Blurred density for the rest of the particle is also visible.

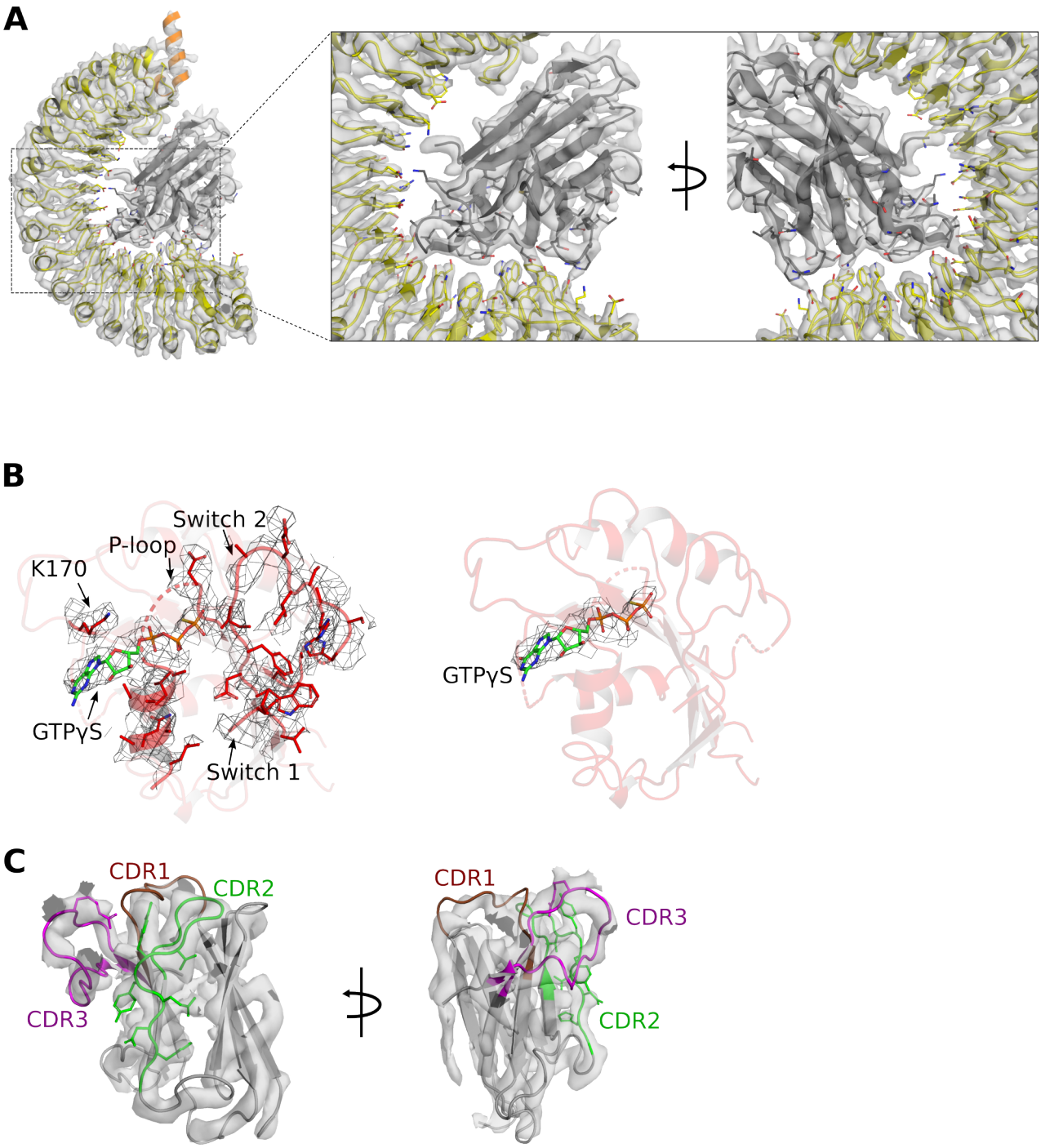

Figure 1 - supplement 4. Quality of the cryo-EM map of CtRoco-Nb$_{Roco1}$-Nb$_{Roco2}$. (A) Map focused on the N-terminal (LRR) domain in complex with Nb$_{Roco2}$. The inset shows a zoom-in on the Nb$_{Roco2}$ binding region. **(B)** Mesh representation of the cryo-EM map around the nucleotide-binding region of the Roc domain (*left*) and around the bound GTPγS molecule (*right*). **(C)** Cryo-EM map around Nb$_{Roco1}$ in two orientations. The CDR loops are highlighted in brown (CDR1), green (CDR2) and magenta (CDR3).

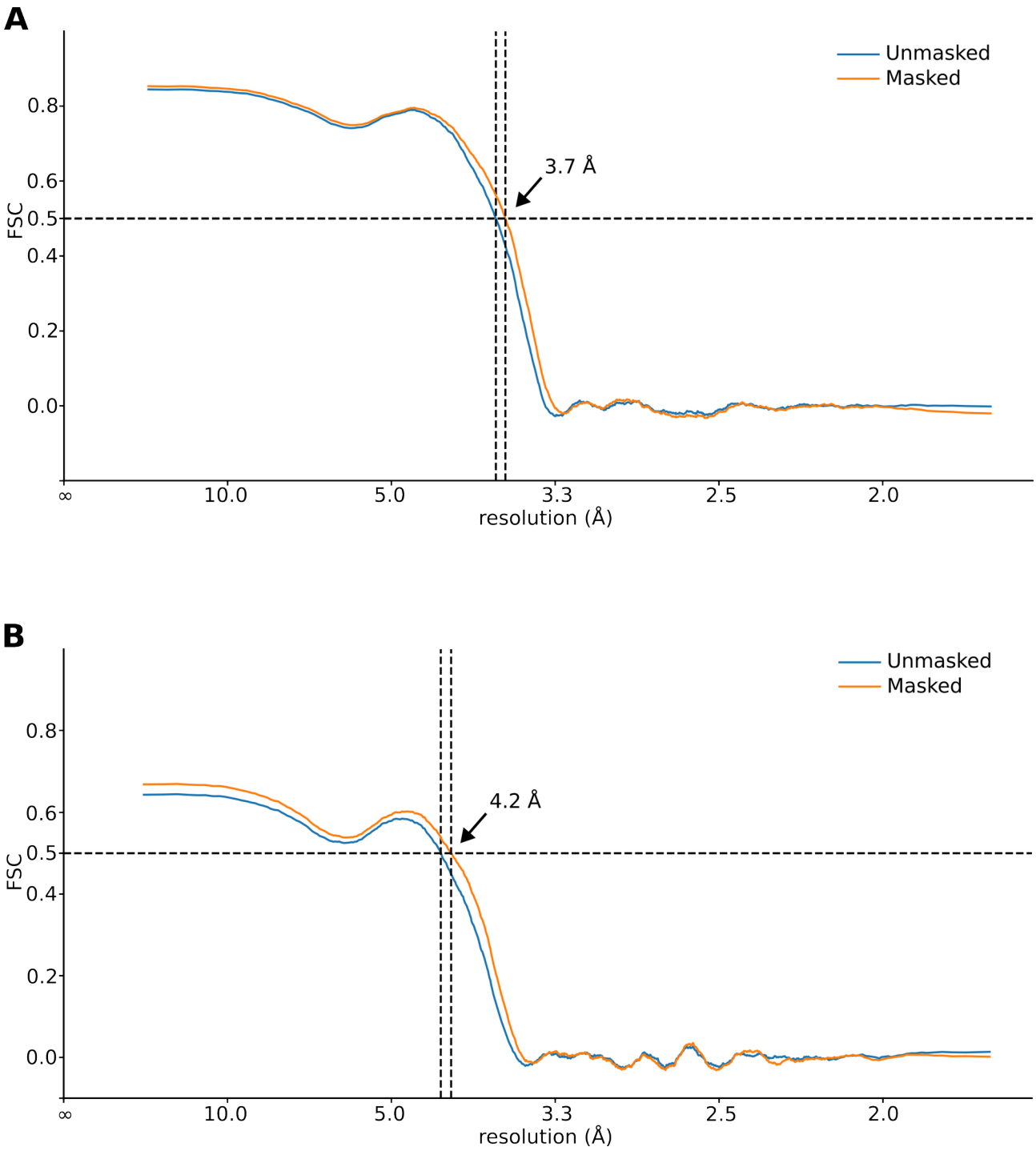

Figure 1 - supplement 5. Fourier shell correlation (FSC) plots of refined atomic models against the focused cryo-EM density maps of CtRoco-Nb$_{Roco1}$-Nb$_{Roco2}$. (A) FSC plot of refined LRR-Nb$_{Roco2}$ model. The resolution at which the FSC curve drops below 0.5 is indicated. **(B)** FSC plot of refined Roc-COR-Nb$_{Roco1}$ model. The resolution at which the FSC curve drops below 0.5 is indicated.

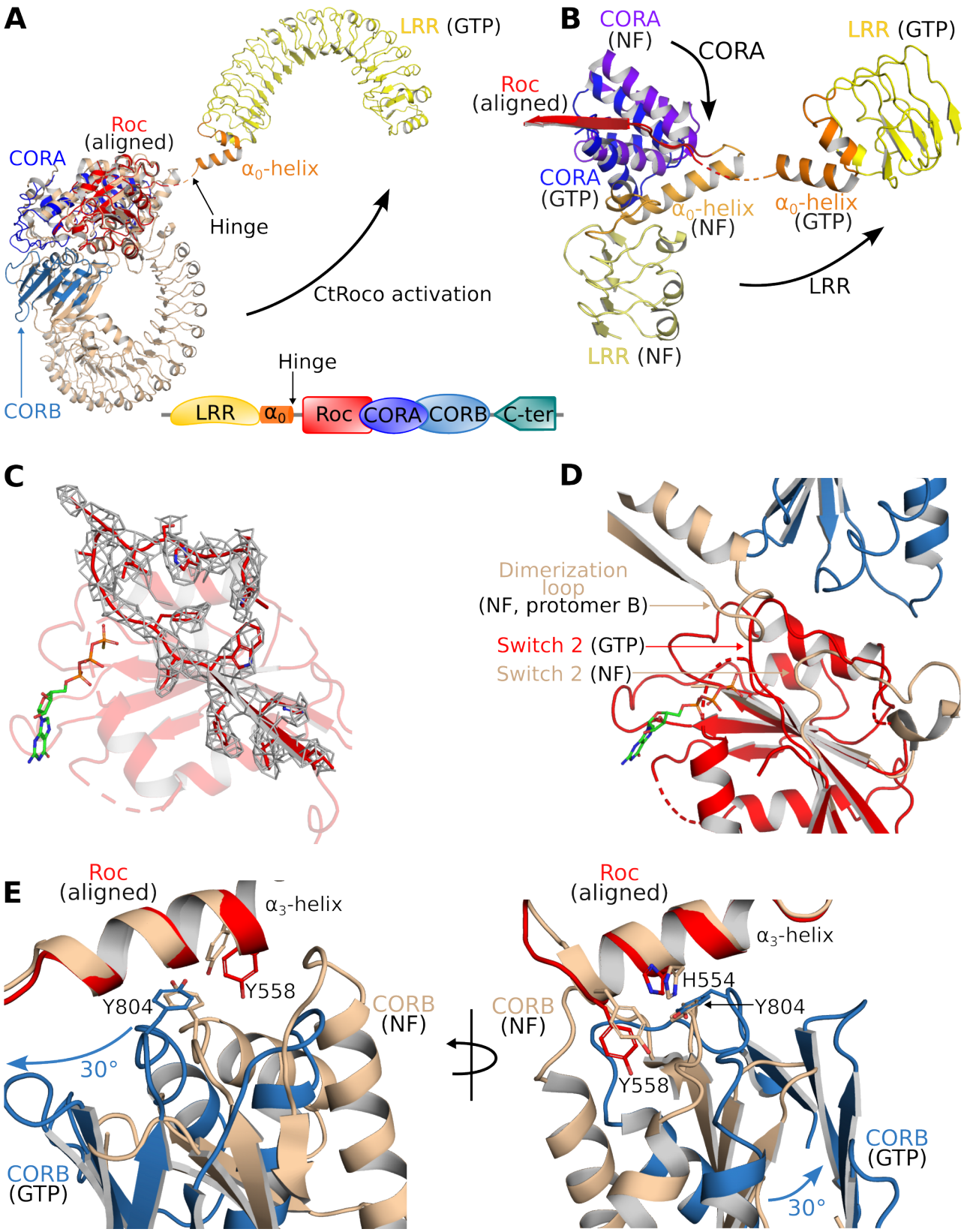

Figure 2. The structural changes occurring upon GTP-driven CtRoco activation. (A) Superposition of a subunit of the nucleotide-free CtRoco dimer (labeled "NF"; beige) and the GTPγS-bound monomeric CtRoco-Nb_{Roco1}-Nb_{Roco2} (labeled "GTP", colored by domain). The Roc domains of both structures were used for the superposition. Nbs were removed in the representation of CtRoco-Nb_{Roco1}-Nb_{Roco2} for clarity. The conformational change occurring in the LRR domain and α_0-helix is indicated by an arrow. **(B)** Close-up

view on the displacement of the LRR, α_0-helix and CORA upon CtRoco activation. The position of CORA in the "GTP" conformation is incompatible with the position of the α_0-helix in the nucleotide-free conformation, providing a mechanism to relay conformational changes from Roc and CORA toward the α_0-helix and LRR domain. The LRR, α_0 and CORA of nucleotide-free and GTPγS-bound CtRoco are colored in different shades of yellow, orange and blue, respectively **(C)** Mesh representation of the cryo-EM map around the Switch 2 region and the preceding β-strand in the GTPγS-bound Roc domain. **(D)** Superposition of Roc domains and surrounding regions of nucleotide-free (beige) and GTPγS-bound CtRoco (colored according to domain). The conformation of the Switch 2 region in GTPγS-bound CtRoco would sterically clash with the "dimerization loop" of the adjacent protomer of the nucleotide-free dimer, providing an initial trigger for nucleotide-induced monomerization. **(E)** Upon activation, the CORB domain of GTPγS-bound CtRoco (blue) displays a 30° rotational movement with regard to corresponding domain of nucleotide-free CtRoco (beige). The H554-Y558-Y804 triad (corresponding to N1437-R1441-Y1699 in LRRK2), located at the Roc-CORB interface, acts as a hinge point for this rotational movement.

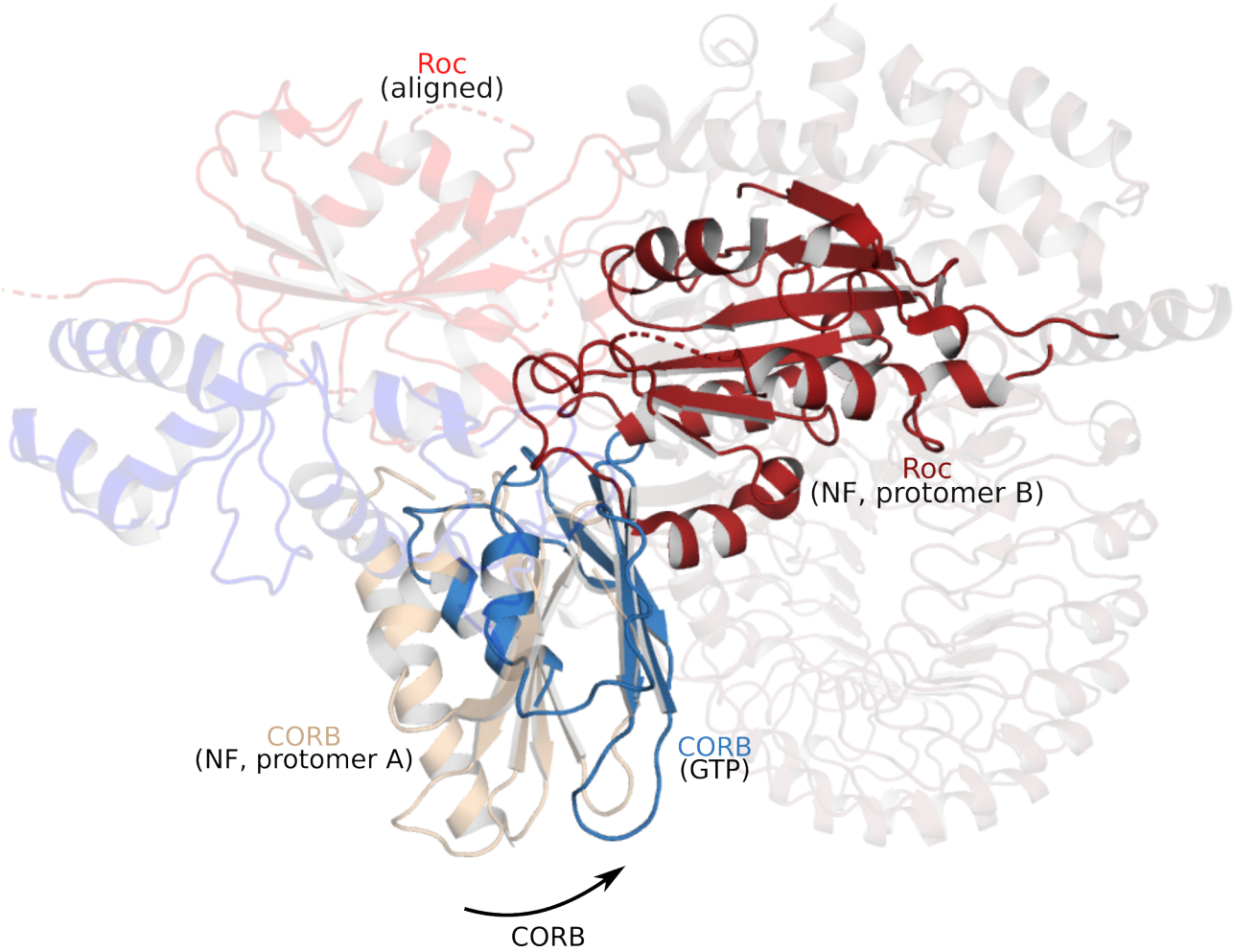

Figure 2 - supplement 1. The rotational movement of the CORB domain upon GTP-driven CtRoco activation induces monomerization. Superposition (on the Roc domain) of a GTPγS-bound CtRoco monomer ("GTP"; colored by domain) on the nucleotide-free CtRoco dimer ("NF", beige). Only the CORB domain of the superposed subunit of nucleotide-free CtRoco is shown for clarity. The rotational movement of the CORB domain upon GTPγS binding would cause sterical clashes with the Roc domain of the adjacent protomer of nucleotide-free CtRoco (brick red), providing a mechanism for monomerization.

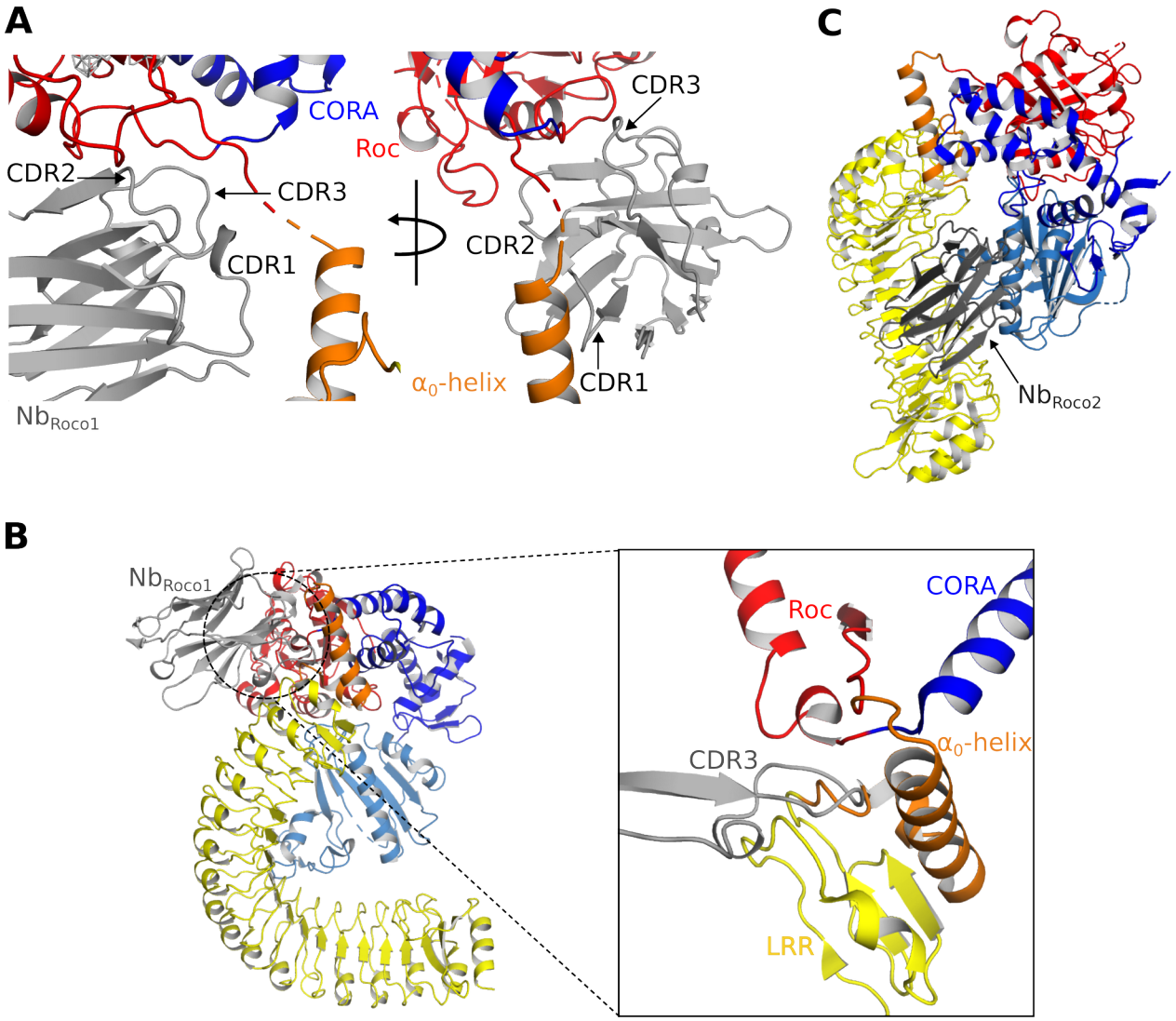

Figure 3. **Mechanisms of the allosteric activation of CtRoco by Nb_{Roco1} and Nb_{Roco2}.** **(A)** Nb_{Roco1} binds at the interface of the Roc, CORA and LRR domains, close to the α_0-helix and the hinge region of the LRR movement. **(B)** Superposition of Nb_{Roco1} on the conformation adopted by the nucleotide-free CtRoco shows considerable sterical clashes between the CDR3 region of Nb_{Roco1} and the LRR domain and α_0-helix of nucleotide-free CtRoco (see inset). This provides a mechanism for the Nb_{Roco1}-mediated stabilization of CtRoco in its GTP-bound active conformation. **(C)** Superposition of Nb_{Roco2} on the conformation adopted by the nucleotide-free CtRoco shows that the position of Nb_{Roco2} in the curvature of the LRR domain is not compatible with the closed conformation of CtRoco, due to severe sterical clashes with the CORB domain.

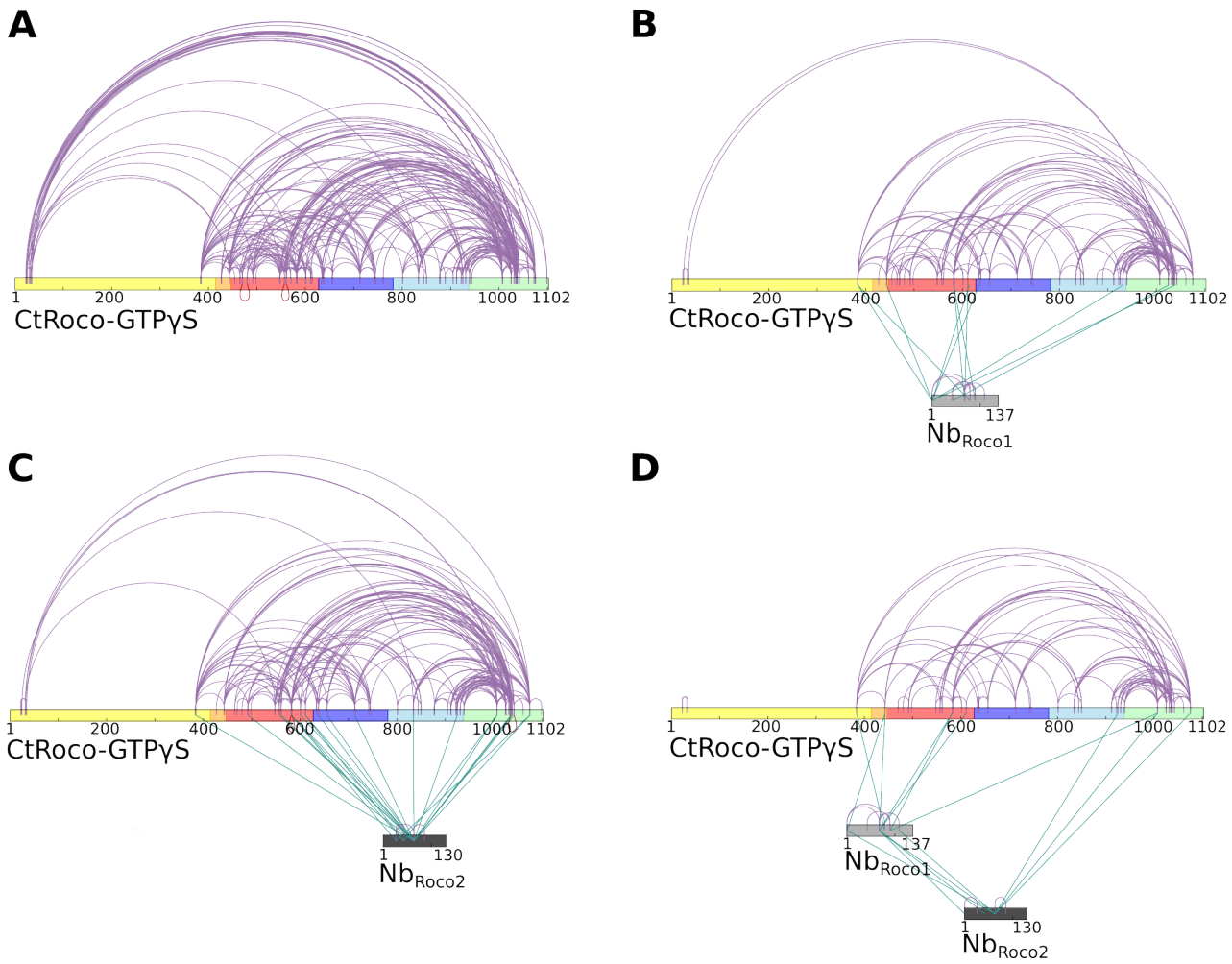

Figure 4. **Cross-linking mass spectrometry (CX-MS) experiments show the stabilization of GTPγS-bound CtRoco in its elongated active conformation by Nb_{Roco1} and/or Nb_{Roco2}. (A)** Intramolecular DSSO-crosslinks within GTPγS-bound CtRoco in the absence of nanobodies. **(B)** Effect of Nb_{Roco1} on the intramolecular DSSO-crosslinks within GTPγS-bound CtRoco. The intermolecular cross-links between CtRoco and Nb_{Roco1} are also shown. **(C)** Effect of Nb_{Roco2} on the intramolecular DSSO-crosslinks within GTPγS-bound CtRoco. The intermolecular cross-links between CtRoco and Nb_{Roco2} are also shown. **(D)** Effect of the combination of Nb_{Roco1} and Nb_{Roco2} on the intramolecular DSSO-crosslinks within GTPγS-bound CtRoco. The intermolecular cross-links between CtRoco, Nb_{Roco1} and Nb_{Roco2} are also shown.

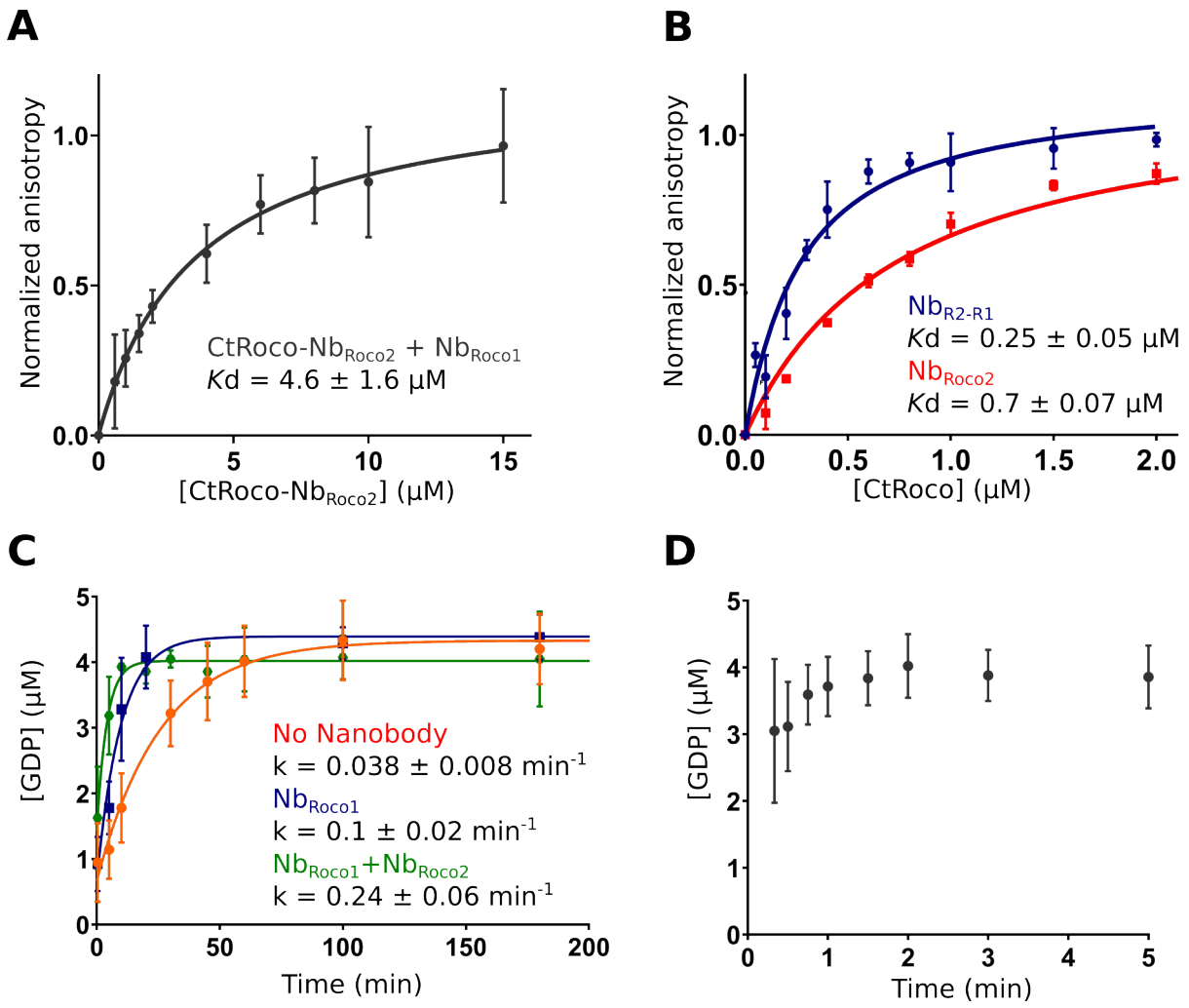

Figure 5. Nb$_{Roco1}$ and Nb$_{Roco2}$ have a synergistic effect on CtRoco activation that is potentiated by the bivalent nanobody construct Nb$_{R2-R1}$. (A) Nb$_{Roco2}$ enables the binding of Nb$_{Roco1}$ to the nucleotide-free CtRoco. The fluorescence anisotropy signal of the FITC-labelled Nb$_{Roco1}$ is monitored upon titration with increasing concentrations of nucleotide-free CtRoco in presence of an excess of Nb$_{Roco2}$. The equilibrium dissociation constant (Kd ± standard error), obtained by fitting of triplicated data with a quadratic binding equation, is given. **(B)** Nb$_{R2-R1}$ has a 3-fold increased affinity towards nucleotide-free CtRoco in comparison to Nb$_{Roco2}$. FITC-labelled Nb$_{R2-R1}$ or Nb$_{Roco2}$ were titrated with nucleotide-free CtRoco, and fluorescence anisotropy data was analyzed as in (A). **(C)** Single turn-over GTP (5μM) hydrolysis rate of CtRoco-L487A (5 μM) in absence of nanobodies (orange), or in presence of either Nb$_{Roco1}$ (blue) or both Nb$_{Roco1}$ and Nb$_{Roco2}$ (green). **(D)** Single turn-over GTP (5 μM) hydrolysis of CtRoco-L487A (5 μM) in presence of Nb$_{R2-R1}$, all GTP was converted within the dead time (20s) of the experiment.

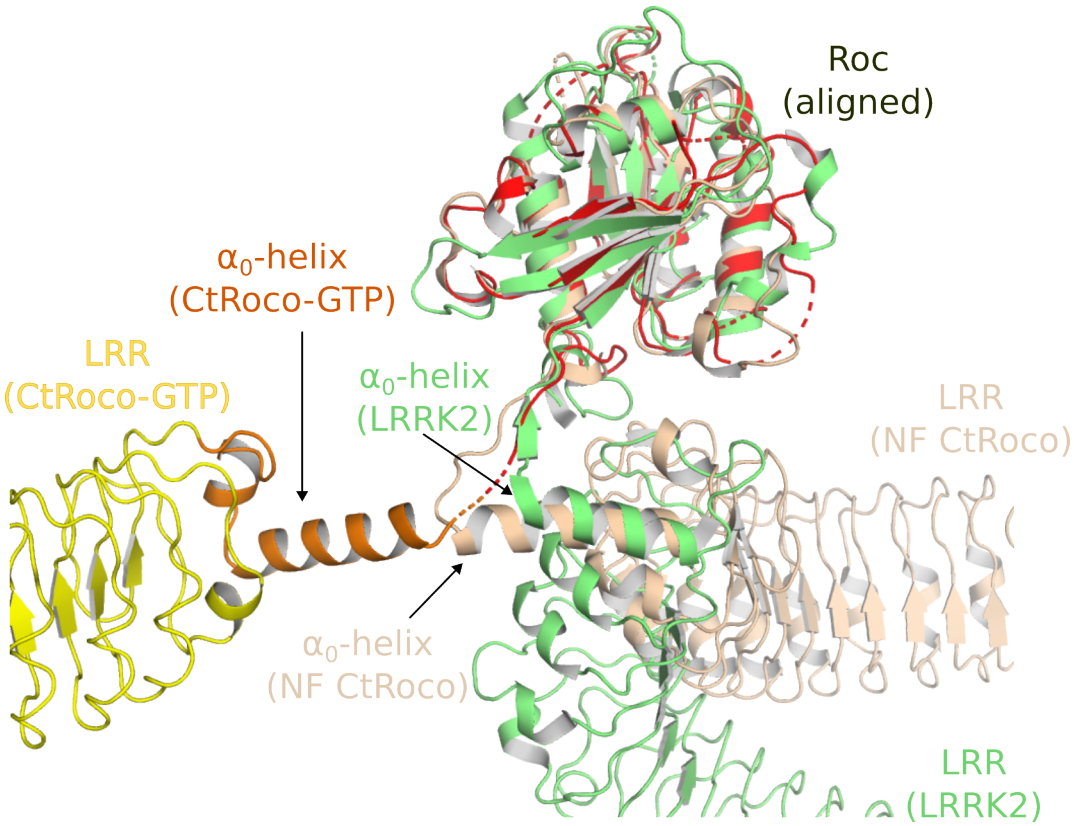

Figure 6. Similarities in the activation mechanisms of CtRoco and LRRK2. Comparison of the conformation of the LRR domain and the α_0-helix adopted within GTPγS-bound CtRoco-Nb_{Roco1}-Nb_{Roco2} (this work, colored by domain), nucleotide-free CtRoco (beige) (PDB: 6hlu) (Deyaert et al., 2019), and GDP-bound LRRK2 (green) (PDB: 7lhw) (Myasnikov et al., 2021). The Roc domain of the three structures was used for the superposition.